1 **Comparative clumped isotope temperature relationships in freshwater carbonates**

2 **Alexandrea Arnold[1,3]*, John Mering[4], Lauren Santi[2-4], Cristian Román-Palacios[3], Huashu**
3 **Li[5], Victoria Petryshyn[6], Bryce Mitsunaga[4], Ben Elliott[4], John Wilson[4], Jamie Lucarelli[3-4],**
4 **Ronny Boch[7], Daniel Ibarra[8], Lin Li[11], Majie Fan[9], Darrell Kaufman[10], Andrew Cohen[11],**
5 **Rob Dunbar[12], James Russell[8], Stefan Lalonde[13], Priyadarsi D. Roy[14], Martin Dietzel[7],**
6 **Xingqi Liu[5], Fengming Chang[15], Robert A. Eagle[1,3,13,16], and Aradhna Tripati[1-4,13,16]**

7 [1]Department of Atmospheric and Oceanic Sciences, University of California, Los Angeles,
8 California, USA, Math Science Building, 520 Portola Plaza, Los Angeles, CA 90024, USA

9 [2]Institute of the Environment and Sustainability, University of California, Los Angeles, LaKretz
10 Hall, 619 Charles E Young Dr E #300, Los Angeles, CA 90024, USA

11 [3]Center for Diverse Leadership in Science, University of California, Los Angeles, California,
12 USA, 595 Charles E Young Dr E, Los Angeles, CA 90024, USA

13 [4]Department of Earth, Planetary, and Space Sciences, University of California, Los Angeles, 595
14 Charles E Young Dr E, Los Angeles, CA 90024, USA

15 [5]College of Resource Environment & Tourism, Capital Normal University, Beijing 100048,
16 China

17 [6]Environmental Studies Program, University of Southern California, Los Angeles, CA, 3454
18 Trousdale Pkwy CAS 106, Los Angeles, CA 90089-0740

19 [7]Institut für Angewandte Geowissenschaften, Technische Universität Graz, Rechbauerstraße 12,
20 8010 Graz, Austria

21 [8]Earth, Environmental, and Planetary Sciences, Brown University, 324 Brook Street, Providence,
22 RI, 02906

23 [9]Department of Earth and Environmental Sciences, University of Texas at Arlington, Arlington,
24 Texas 76019, USA

25 [10]School of Earth and Sustainability, Northern Arizona University, S San Francisco St, Flagstaff,
26 AZ 86011

27 [11]Department of Geosciences, University of Arizona, 1040 E. 4th Street Tucson, AZ 85721

28 [12]Department of Earth System Science, Stanford University, 473 Via Ortega, Building Y2E2,
29 Stanford, CA 94305, USA

30 [13]University of Brest, Brest, France, UMR 6538 Laboratoire Géosciences Océan, Institut
31 Universitaire Européen de la Mer, Technopôle Brest-Iroise, Place Nicolas Copernic, Plouzané
32 29280, Brest, France

33 [14]Instituto de Geología, Universidad Nacional Autónoma de México (UNAM), Ciudad
34 Universitaria, 04510 Ciudad de México, México

35 [15]Key Laboratory of Marine Geology and Environment, Institute of Oceanology, Chinese
36 Academy of Sciences, Qingdao 266071, China

37   [16]School of Earth Sciences, School of Geographical Sciences, University of Bristol, Bristol, BS8
38   1QU, United Kingdom
39

40   Corresponding author: Alexandrea Arnold (ajarnold1@g.ucla.edu) and Aradhna Tripati
41   (atripati@g.ucla.edu)

42   **Key Points:**

43   • Δ_{47} calibration dataset for 135 freshwater carbonate samples shows evidence for material-
44   specificity in Δ_{47}-temperature dependence.

45   • Δ_{47}-derived estimates of source water $\delta^{18}O$ usually within 2‰ of modern values.

46   • We evaluate the impact of calibrations and predictions on paleotemperature
47   reconstructions.

Abstract

49   Lacustrine, riverine, and spring carbonates are archives of terrestrial climate change and are
50   extensively used to study paleoenvironments. Clumped isotope thermometry has been applied to
51   freshwater carbonates to reconstruct temperatures, however, limited work has been done to
52   evaluate comparative relationships between clumped isotopes and temperature in different types
53   of modern freshwater carbonates. Therefore, in this study, we assemble an extensive calibration
54   dataset with 135 samples of modern lacustrine, fluvial, and spring carbonates from 96 sites and
55   constrain the relationship between independent observations of water temperature and the
56   clumped isotopic composition of carbonates (denoted by Δ_{47}). We restandardize and synthesize
57   published data and report 159 new measurements of 25 samples. We derive a composite
58   freshwater calibration and also evaluate differences in the Δ_{47}-temperature dependence for
59   different types of materials to examine whether material-specific calibrations may be justified.
60   When material type is considered, there is a convergence of slopes between biological carbonates
61   (freshwater gastropods and bivalves), micrite, biologically-mediated carbonates (microbialites
62   and tufas), travertines, and other recently published syntheses, but statistically significant
63   differences in intercepts between some materials, possibly due to seasonal biases, kinetic isotope
64   effects, and/or varying degrees of biological influence. Δ_{47}-based reconstructions of water $\delta^{18}O$
65   generally yield values within 2‰ of measured water $\delta^{18}O$ when using a material-specific
66   calibration. We explore the implications of applying these new calibrations in reconstructing
67   temperature in three case studies.

1 Introduction

69   Paleoenvironmental reconstructions from freshwater sediments can be used to enhance
70   our understanding of ecosystem and climate change both within the aquatic systems and their
71   proximal terrestrial environments (e.g., Brenner et al., 1999; Xu et al., 2006)). Carbonate-bearing
72   sediments deposited in freshwater systems are widespread and are sensitive to changes in the
73   local environment, tectonic setting, and hydrological conditions, and thus provide a promising
74   archive of continental paleoclimatic information (Arenas-Abad et al., 2010; Gierlowski-
75   Kordesch, 2010; Hren & Sheldon, 2012). However, quantitative terrestrial temperature proxies
76   that can be applied to carbonate sediments are relatively scarce. Of the multiple proxies that have
77   been used to estimate terrestrial temperatures with varying degrees of uncertainty, including soil
78   carbonates, speleothems, fracture veins, ostracods, trace element ratios in lacustrine sediments,
79   tree rings, leaf margin analysis, pollen, biomarkers, and noble gasses in groundwater (Boch et al.,
80   2019; Esper et al., 2018; Gallagher & Sheldon, 2013; Kaufman et al., 2020; Meckler et al., 2021;
81   Powers et al., 2010; Stute & Schlosser, 2000; Wilf, 1997; Wrozyna et al., 2022), only the first
82   five types of proxies are carbonate-associated.

83   However, work has shown that multiply-substituted carbonate "clumped" isotope
84   thermometry presents a promising proxy for reconstructing temperature, based on the
85   thermodynamic exchange of isotopes between isotopologues of carbonate-containing groups
86   (Ghosh, Adkins, et al., 2006; Hill et al., 2014; Schauble et al., 2006; Tripati et al., 2015) with
87   widespread applicability in paleoclimatic, paleohydrological, and paleoelevation contexts (e.g.
88   Csank et al., 2011; Eagle et al., 2013; Hren et al., 2013; Huntington et al., 2010, 2015;
89   Huntington & Lechler, 2015; Santi et al., 2020; Tripati et al., 2010, 2014). Theoretical
90   calculations indicate that measurements of clumped isotopes can be used for paleothermometry
91   because at equilibrium, the abundance of the multiply-substituted isotopologue $^{13}C^{18}O^{16}O_2$ in

92 carbonates is related solely to the formation temperature of the mineral (Ghosh, Adkins, et al.,
93 2006; Hill et al., 2014; Schauble et al., 2006; Tripati et al., 2015), with cooler temperatures
94 favoring enhanced "clumping" of heavy isotopes within the mineral lattice (e.g., the forward
95 reaction in Equation 1).

96

97 $$Ca^{12}C^{18}O^{16}O_2 + Ca^{13}C^{16}O_3 \rightarrow Ca^{13}C^{18}O^{16}O_2 + Ca^{12}C^{16}O_3 \qquad (1)$$
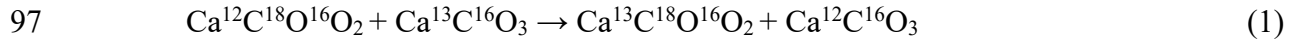
98

99 We report the abundance of mass-47 CO_2 liberated from carbonate minerals digested in
100 phosphoric acid (δ_{47}) compared to a randomized (stochastic) distribution of clumping in a
101 sample. This excess of $^{13}C^{18}O^{16}O$ is denoted as Δ_{47} in Equation 2, where $R^i = $ (mass i/mass 44):

102

103 $$\Delta_{47}\,(‰) = [(R^{47}/(R^{47}_{stochastic}) - 1) - (R^{46}/(R^{46}_{stochastic}) - 1) - (R^{45}/(R^{45}_{stochastic}) - 1)] \times 1000 \qquad (2)$$

104

105 An advantage of carbonate clumped isotope derived temperature estimates is that they are
106 independent of the $^{18}O/^{16}O$ ratio ($\delta^{18}O$) of the precipitating fluid, as the relevant isotope
107 exchange reaction (Equation 1) takes place within a single phase. Carbonate $\delta^{18}O$ ratios are
108 simultaneously measured during clumped isotope analysis and can be combined with
109 temperature estimates obtained from Δ_{47} analysis to calculate $\delta^{18}O$ values of water at the time of
110 carbonate formation (Epstein et al., 1953; Urey, 1947; Vasconcelos et al., 2005).

111 Clumped isotopes have been previously used to constrain past lake and river water
112 temperature (Cheng et al., 2022; Horton et al., 2016; Hudson et al., 2017; Huntington et al.,
113 2010, 2015; Kele et al., 2015; H. Li et al., 2021; Petryshyn et al., 2015; L. M. Santi et al., 2020;
114 Wang et al., 2021). The additional temperature constraint provided from Δ_{47} measurements
115 allows for a calculation of the $\delta^{18}O$ of meteoric waters, which can provide constraints on past
116 hydrology. The Δ_{47}-temperature and Δ_{47}-derived water $\delta^{18}O$ in freshwater carbonates and other
117 types of terrestrial archives have in turn been used to evaluate process depiction in climate
118 models (Cheng et al., 2022; Eagle, Risi, et al., 2013; L. M. Santi et al., 2020; Tripati et al., 2014),
119 constrain hydrologic parameters (L. M. Santi et al., 2020), and to constrain paleoaltimetry (e.g.,
120 Ghosh, Garzione, et al., 2006; Huntington et al., 2010, 2015; Ingalls et al., 2017; L. Li et al.,
121 2019).

122 However, the accuracy of these reconstructions is fundamentally underpinned by the
123 calibration(s) used for calculations. The body of literature for clumped isotope measurements of
124 modern lacustrine and riverine samples is limited. Only four studies have reported Δ_{47}-T
125 calibrations (Anderson et al., 2021; Kato et al., 2019; Kele et al., 2015; H. Li et al., 2021), with
126 three calibrations being solely derived from freshwater sediments (H. Li et al., 2021: n=33, Kele
127 et al. 2015: n = 24, Kato et al. 2019: n=33). Most clumped isotope studies of freshwater
128 carbonates have analyzed a small number of samples (Anderson et al., 2021; Grauel et al., 2016;
129 Horton et al., 2016; Hudson et al., 2017; Huntington et al., 2010, 2015; Kato et al., 2019; Kele et
130 al., 2015; H. Li et al., 2021; Petryshyn et al., 2015; L. M. Santi et al., 2020; Wang et al., 2021).
131 Of these 11 studies reporting data for modern freshwater carbonates, five report new data for <5
132 samples, while eight have data for <11 samples, and the remaining four have data consisting of
133 25-33 samples. The smaller size of these prior datasets on clumped isotope compositions means

134   that the community has not been able to explore in detail the potential for material-specific
135   calibrations, possible influences of seasonal and temperature bias in carbonate formation, and
136   non-equilibrium kinetic or pH dependent effects which could differentially affect different types
137   of carbonates.

138   Recent work to constrain the Δ_{47}-temperature relationship has suggested that all
139   carbonates have the same temperature dependence (i.e., calibration slope), but the calibration
140   intercept may differ due to mineral-specific phosphoric acid fractionation factors (Müller et al.,
141   2019; van Dijk et al., 2019). Recent efforts have advanced practices and improved
142   interlaboratory consistency (Anderson et al., 2021; Bernasconi et al., 2021; Daëron et al., 2016;
143   Petersen et al., 2019; Upadhyay et al., 2021), and use of consistent approaches for
144   standardization and isotope ratio calculations have reduced many offsets (e.g., Petersen et al.,
145   2019). Petersen et al. (2019) reprocessed 14 calibration studies, encompassing synthetic and
146   natural carbonates, using updated parameter values for clumped isotope calculations and found
147   that use of the IUPAC parameters with identical data processing resulted in increased agreement
148   between calibration lines and a convergence of slopes within many of the individual studies.
149   From this synthesis, the authors proposed a 'universal', in which one calibration is derived and
150   applied for all carbonate types. However, it has been acknowledged that it is uncertain if only
151   one relationship exists, since despite improvements in data processing and standardization
152   procedures, differences are still observed (Petersen et al., 2019). Recently, the "InterCarb"
153   project defined new, community-based standard values for carbonate clumped isotope
154   standardization, as well as proposed a new reference frame (I-CDES), which has been shown to
155   help resolve inter-laboratory differences (Bernasconi et al., 2021). The application of carbonate
156   standardization and newly defined carbonate standard values, in concert with developments in
157   data handling procedures (Daëron, 2021), to reprocessed data from four older calibration studies
158   has been shown to help resolve the disagreement between their derived calibration lines
159   (Anderson et al., 2021).

160   A few studies have suggested statistically significant differences between calibrations
161   using different types of carbonates (Davies & John, 2019; Eagle, Eiler, et al., 2013; Henkes et
162   al., 2013; Kele et al., 2015; Kimball et al., 2016; Müller et al., 2019). Factors such as seasonality
163   of carbonate growth, the ecology of shell forming organisms, and kinetic isotope effects relating
164   to different processes in mineral formation have been shown to broadly influence empirical
165   relationships between Δ_{47} measurements and environmental parameters, including in corals (eg.
166   Ghosh, Adkins, et al., 2006; Kimball et al., 2016; Saenger et al., 2012; Spooner et al., 2016),
167   echinoids (Davies & John, 2019), terrestrial gastropods (eg. Dong et al., 2021; Eagle, Eiler, et al.,
168   2013; Zaarur et al., 2013), as well as synthetic carbonates (eg. Tang et al., 2014; Tripati et al.,
169   2015), with studies of slow growing cave carbonates indicating that many if not most carbonates
170   could express a degree of kinetic isotope effect (Daëron et al., 2019; Kluge et al., 2014; Tripati et
171   al., 2015).

172   In this work, we discuss clumped isotope data from 135 samples collected from 96 sites
173   in modern lakes, rivers, and springs. At present, due to limited freshwater calibration data, it is
174   unresolved whether the differences in calibration relationships between different types of
175   freshwater carbonate materials exist, and whether synthetically-derived regression parameters are
176   appropriate to use in freshwater samples that are field-collected. The recently published
177   syntheses from Petersen et al. (2019) had no freshwater carbonates, and Anderson et al. (2021)
178   had 16 carbonates (tufas and travertines) of which 7 were between T < 10 ºC, and 6 were T > 30

179 °C. This study augments the literature with 159 new clumped isotope measurements for 25 sites,
180 and additionally incorporates measurements from published datasets, including samples from 59
181 sites that have been recalculated on the new reference frame (Bernasconi et al., 2021). It includes
182 pairs of measurements from 12 sites that have been recently reanalyzed (Anderson et al., 2021)
183 and are recalculated on the new reference frame.

184 This dataset allows us to investigate clumped isotope signatures in travertines, micrites,
185 biotic (freshwater mollusks), and biologically mediated (tufas and microbialites) phases of
186 freshwater carbonate in order to provide a foundation for intercomparison and calibration of
187 carbonate clumped isotope results from freshwater systems. Sample localities within this study
188 are geographically diverse, and include equatorial, mid-latitude, and polar sites at a variety of
189 elevations and climates. We evaluate the seasonality of carbonate formation, and present a
190 composite freshwater calibration and material-specific calibrations. We assess the potential of
191 this proxy to robustly reconstruct water temperature and source water $\delta^{18}O$ in both modern and
192 past contexts.

193 **2 Materials and Methods**

194 2.1 Sample and site selection

195 Samples included in this study are from modern lakes (including playas), rivers, and
196 springs, from geographically and climatically diverse settings (Figure 1; Table 1). Carbonate
197 materials included in this dataset were selected to represent modern lacustrine surface-water
198 conditions. For lakes, biogenic and biologically-mediated samples selected for analysis are types
199 that grow nearshore, or occupy the photic zone above the thermocline; we also selected
200 endogenic carbonate because formation occurs in surface waters, where evaporation and
201 photosynthesis have the strongest effect on water chemistry (Gierlowski-Kordesch, 2010; Hren
202 & Sheldon, 2012; Platt & Wright, 2009).

203 For this work, we only included localities where modern surface water temperatures have
204 been measured (Supplementary Table 1). For sites where multiple years of hydrographic data are
205 available, we report temperature variability of one standard deviation of the monthly average
206 temperatures during the typical season of carbonate formation for each type of carbonate (see
207 Section 3.1). In sites where the average modern water temperature during the interval of
208 carbonate growth was limited to data from a short time interval (i.e., less than one year), given
209 that there is year-to-year variability in temperatures, we report a temperature uncertainty of two
210 standard deviations of the available measurements. Some sites within our study are less studied,
211 and if there was limited temperature information for the water body, such as a 'summer' average,
212 or the site has a measured temperature value but uncertainty was not reported, we use the
213 average standard deviation for well constrained sample sites in our study (± 2°C).

214
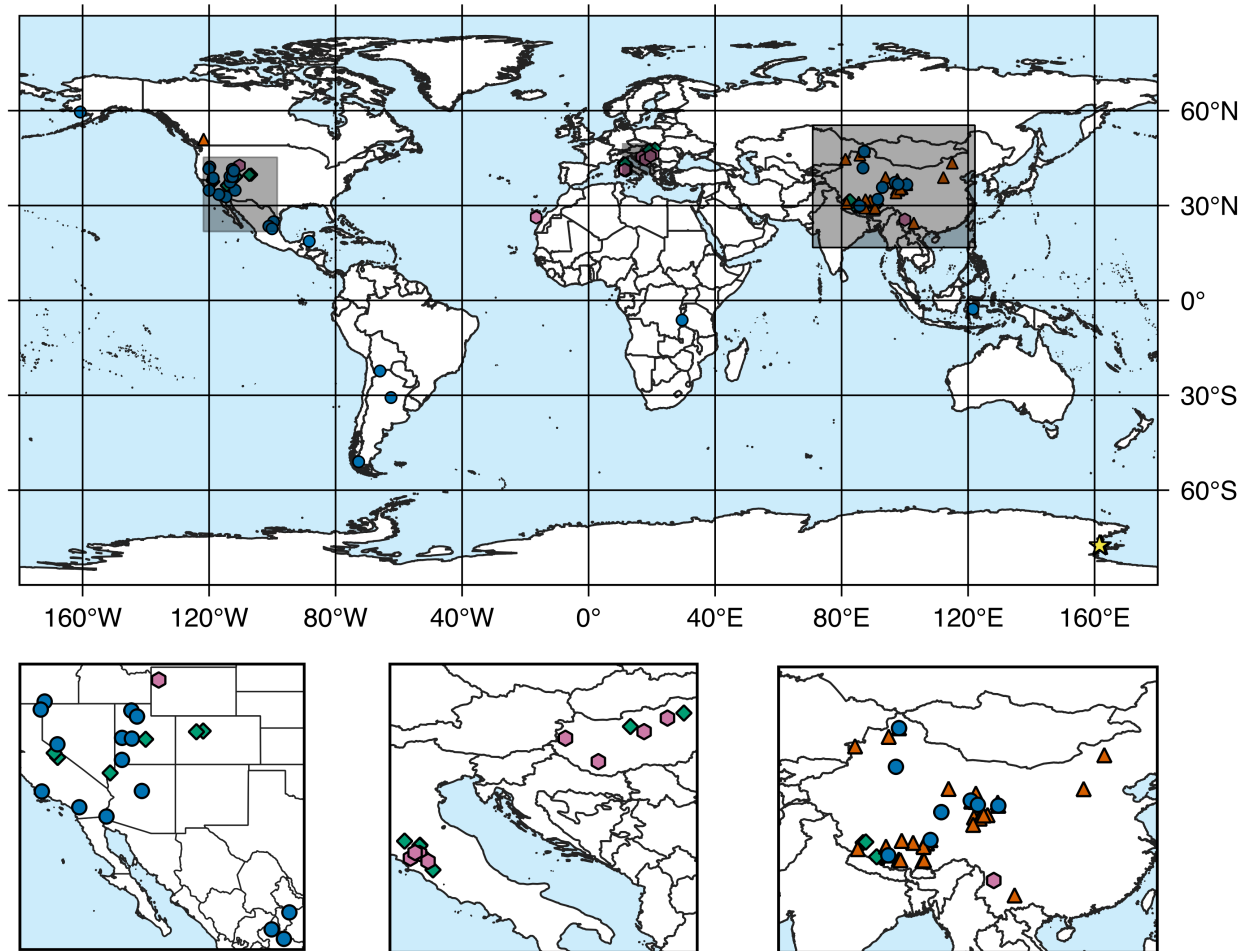
Figure 1: Sample locations used for this study. We discuss clumped isotope data from 135 samples collected from 96 sites in modern lakes, rivers, and springs. Blue circles indicate location of samples with new data from the Eagle-Tripati lab (n = 25; 159 measurements), orange triangles indicate data measured in the Eagle-Tripati lab that has been published and was recalculated onto the I-CDES reference frame for this study (n = 30), green diamonds indicate data from other labs that were recalculated onto the I-CDES reference frame as part of this study (n = 29), pink hexagons denotes sites where samples were analyzed twice, with one set of measurements being recalculated and the other taken directly from published data (n = 12), yellow stars represent data directly taken from other publications (n = 3).

Sample name	Latitude	Longitude	MAAT (°C)	Water temperature (°C)	1 s.d. (°C)	$\delta^{13}C$ (‰, VPDB)	$\delta^{18}O$ (‰, VPDB)	Δ_{47} (‰, I-CDES)	1 s.e.	Data source
Bivalves										
Red Rock	34.8	-111.8	15.3	16.4	1.0	-10.0	-12.0	0.617	0.012	Eagle-Tripati lab (this study)
Colorado River	32.7	-114.7	21.9	20.8	1.3	-9.1	-13.0	0.604	0.016	Eagle-Tripati lab (this study)
Vail Lake	33.5	-117.0	12.3	24.5	1.5	-6.6	-1.1	0.589	0.014	Eagle-Tripati lab (this study)
Wulungu Lake	47.1	87.2	7.0	21.7	2.5	-3.6	-4.3	0.611	0.002	Eagle-Tripati lab (this study)
Gastropods										
Santa Clara River	37.4	-113.5	15.3	13	3.1	-7.1	-14.0	0.619	0.010	Eagle-Tripati lab (this study)
Painter Spring	39.2	-113.4	11.8	12.5	3.1	-10.2	-13.2	0.627	0.007	Eagle-Tripati lab (this study)
Lake Warner	42.2	-119.8	8.3	20	2.0	-10.6	-8.9	0.596	0.006	Eagle-Tripati lab (this study)
Clear Lake	39.1	-112.6	10.4	15	3.0	-7.0	-14.2	0.616	0.002	Eagle-Tripati lab (this study)
Lake Tanganyika	-6.2	29.6	22.3	26.9	2.0	-0.4	1.9	0.581	0.007	Eagle-Tripati lab (this study)
Lake Towuti	-2.8	121.5	23.6	29	1.0	-7.6	-7.2	0.573	0.003	Eagle-Tripati lab (this study)
Nimgun Lake	59.6	-160.8	-1.3	8	3.1	-6.1	-12.2	0.641	0.004	Eagle-Tripati lab (this study)
Fuxian Lake	24.4	102.9	17.3	17.9	3.8	-2.2	-3.5	0.608	0.004	Eagle-Tripati lab[a]
Lake Manasarovar	30.7	81.6	4.0	12.8	2.0	-3.8	-3.3	0.638	0.009	Eagle-Tripati lab[a]
Yamdrok Yumco	29.1	90.4	5.0	11.9	1.5	-6.2	-11.2	0.643	0.010	Eagle-Tripati lab[a]
Yamdrok Yumco	29.2	90.6	5.0	7	1.5	-0.4	-4.5	0.643	0.006	Eagle-Tripati lab[a]
Tso Nag	31.6	82.3	-1.3	12.8	2.0	-2.6	-5.7	0.621	0.010	Eiler lab[b]
Tsangpo	29.6	84.9	-2.4	12.8	2.0	-4.1	-15.9	0.621	0.010	Eiler lab[b]
Zhongba	29.7	84.2	-2.6	12.8	2.0	-5.3	-13.5	0.629	0.011	Eiler lab[b]
Bosten Lake	41.9	86.8	9.5	22.9	2.5	-3.9	-2.4	0.611	0.008	Eagle-Tripati lab (this study)
Cuona Lake	32.0	91.5	-1.1	15.7	2.5	-1.1	-7.1	0.629	0.009	Eagle-Tripati lab (this study)
Dajia Co	29.9	85.7	-2.9	9.8	2.5	0.0	-4.5	0.627	0.005	Eagle-Tripati lab (this study)
Jinzihai Lake	36.7	97.9	4.3	17.4	2.5	-10.5	-8.0	0.596	0.005	Eagle-Tripati lab (this study)
Wulungu Lake	47.1	87.2	7.0	21.7	2.5	-2.3	-3.1	0.613	0.010	Eagle-Tripati lab (this study)
Micrite										
Laguna Pozuelos	-22.4	-66.0	8.6	14.6	2.0	-7.4	0.4	0.625	0.012	Eiler lab (this study)
Mar Chiquita	-30.8	-62.5	18.4	29	2.0	-3.2	-1.1	0.611	0.004	Eiler lab (this study)
El Potosi	24.8	-99.7	21.8	23.6	3.1	-5.3	-7.7	0.599	0.002	Eagle-Tripati lab[c]
Kusai	35.7	92.9	-4.4	10.5	2.0	3.1	-0.4	0.642	0.003	Eagle-Tripati lab[c]
Laguna La Salada	23.4	-101.1	14.9	23	3.1	3.3	0.0	0.616	0.001	Eagle-Tripati lab[c]
Laguna Las Cruces	22.7	-100.1	20.9	19	3.1	-0.7	-4.0	0.625	0.002	Eagle-Tripati lab[c]
Zaca Lake	34.8	-120.0	13.3	25	2.0	1.5	-1.6	0.598	0.005	Eagle-Tripati lab[c]
Pipahai Lake	38.9	112.2	4.1	19.3	2.6	1.7	-2.5	0.627	0.015	Eagle-Tripati lab[c]
Chagan Lake	43.4	115.0	1.9	24	2.6	-2.4	-4.8	0.624	0.010	Eagle-Tripati lab[c]
Gahai Lake	37.0	100.6	1.3	15.8	2.5	2.2	2.0	0.637	0.004	Eagle-Tripati lab[c]

Qinghai Lake	36.6	100.7	1.9	19.3	2.6	2.9	2.3	0.652	0.007	Eagle-Tripati lab[c]
Kuhai Lake	35.3	99.2	-5.1	12.5	2.5	2.1	1.4	0.682	0.001	Eagle-Tripati lab[c]
Eling Lake	35.0	97.7	-4.3	14	2.6	-1.0	-4.3	0.655	0.006	Eagle-Tripati lab[c]
Zhaling Lake	35.0	97.4	-5.9	16.9	2.6	0.5	-2.7	0.611	0.001	Eagle-Tripati lab[c]
Xingxinghai Lake	34.9	98.1	-2.7	15.7	2.6	-0.1	-4.4	0.620	0.012	Eagle-Tripati lab[c]
Koucha Lake	34.0	97.2	-5.3	12.5	2.5	4.6	-5.1	0.638	0.003	Eagle-Tripati lab[c]
Donggi Cona Lake	35.3	98.7	-1.7	11.3	2.5	1.7	-4.7	0.637	0.013	Eagle-Tripati lab[c]
Gahai Lake2	37.1	97.6	5.4	18.3	2.5	1.6	0.0	0.605	0.011	Eagle-Tripati lab[c]
Tuosu Lake	37.2	97.0	5.0	17.7	2.5	1.5	-1.3	0.616	0.013	Eagle-Tripati lab[c]
Hala Lake	38.2	97.6	-4.1	14	2.6	3.9	1.0	0.657	0.008	Eagle-Tripati lab[c]
Cuona Lake	32.0	91.5	-1.1	15.7	2.6	2.2	-9.5	0.643	0.004	Eagle-Tripati lab[c]
Pung Co	31.5	91.0	0.4	15.7	2.6	4.8	-4.1	0.664	0.003	Eagle-Tripati lab[c]
Jiang Co	31.5	90.8	0.4	13.1	2.5	3.2	-5.6	0.659	0.006	Eagle-Tripati lab[c]
Bam Co	31.2	90.5	-1.7	12	2.5	3.2	-6.2	0.643	0.014	Eagle-Tripati lab[c]
Shen Co	31.0	90.5	-1.7	12.2	2.6	3.9	-5.8	0.656	0.004	Eagle-Tripati lab[c]
Selin Co	31.6	89.1	1.7	12.2	2.6	5.0	-3.5	0.651	0.016	Eagle-Tripati lab[c]
Dagze Co	31.8	87.6	1.0	12.2	2.6	2.0	-8.6	0.653	0.009	Eagle-Tripati lab[c]
Zharinanmu Co	31.1	85.4	0.2	14.5	2.6	4.4	-6.6	0.645	0.015	Eagle-Tripati lab[c]
Dajia Co	29.9	85.7	-2.9	9.8	2.6	3.9	-7.4	0.652	0.007	Eagle-Tripati lab[c]
Angrenjin Co	29.3	87.2	2.3	15.7	2.6	0.6	-7.4	0.634	0.020	Eagle-Tripati lab[c]
Lang Co	29.2	87.4	2.3	15.3	2.5	2.9	-5.5	0.634	0.016	Eagle-Tripati lab[c]
Sailimu Lake	44.6	81.2	-1.5	18.7	2.6	2.7	-1.5	0.641	0.009	Eagle-Tripati lab[c]
Ailike Lake	45.9	85.8	7.2	25.6	2.5	-3.1	-6.7	0.596	0.009	Eagle-Tripati lab[c]
Wulungu Lake	47.1	87.2	7.0	21.7	2.6	0.8	-5.1	0.605	0.003	Eagle-Tripati lab[c]
Sugan Lake	38.9	93.9	0.4	15.7	2.6	0.8	4.4	0.645	0.005	Eagle-Tripati lab[c]
Blue Eagle Lake	39.8	-106.8	5.4	15.6	3.1	-4.4	-14.0	0.663	0.014	Eiler lab[d]
Emerald Lake	39.1	-111.5	5.4	12.5	3.1	-0.3	-11.4	0.663	0.011	Eiler lab[d]
South Grizzly Lake	39.7	-107.3	2.5	11.6	3.1	-3.2	-14.1	0.675	0.021	Eiler lab[d]

Microbialites

Laguna Bacalar	18.7	-88.4	27.0	29	2.0	-1.8	-6.0	0.585	0.009	Eagle-Tripati lab (this study)
Lago Sarmiento	-51.1	-72.7	6.5	12.2	2.0	4.9	-1.3	0.633	0.016	Eagle-Tripati lab (this study)
South Arm, Great Salt Lake	41.0	-112.2	8.5	26.1	2.0	3.6	-4.9	0.600	0.003	Eagle-Tripati lab (this study)
North Arm, Great Salt Lake	41.4	-112.7	11.0	27.7	2.0	4.6	-4.8	0.605	0.006	Eagle-Tripati lab (this study)
Kelly Lake	51.0	-121.8	3.5	17	2.0	-2.5	-16.5	0.636	0.006	Eiler lab[e]
Pavillion Lake	50.9	-121.7	3.5	19	2.0	0.6	-11.3	0.630	0.007	Eiler lab[e]

Ooids

South Arm, Great Salt Lake	41.4	-112.7	8.5	27.7	2.0	4.0	-4.4	0.599	0.006	Eagle-Tripati lab (this study)
North Arm, Great Salt Lake	41.0	-112.2	11.0	26.1	2.0	4.3	-4.2	0.603	0.006	Eagle-Tripati lab (this study)

Tufas

Lake Surprise	41.5	-120.1	5.6	19	3.8	3.6	-2.7	0.630	0.005	Eagle-Tripati lab[f]
Walker Lake	38.7	-118.8	13.0	24.1	4.2	0.4	-2.8	0.602	0.003	Eagle-Tripati lab (this study)
Cannatoppa*	43.3	11.6	14.4	11	2.0	-4.0	-5.4	0.653	0.006	Bernasconi lab[g]
						-4.1	-5.4	0.628	0.013	Bergmann lab
La Pigna*	43.1	11.3	14.4	12.5	2.0	-11.3	-5.7	0.643	0.008	Bernasconi lab[g]
						-11.4	-5.5	0.621	0.012	Bergmann lab
Sarteano*	43.0	11.9	14.2	20.7	2.0	0.6	-7.4	0.609	0.006	Bernasconi lab[g]
						0.4	-7.3	0.594	0.012	Bergmann lab
Szalajka	48.1	20.4	9.5	12.1	2.0	-9.4	-9.3	0.666	0.007	Bernasconi lab[g]
Szalajka*	48.1	20.4	9.5	11	2.0	-10.2	-8.5	0.642	0.007	Bernasconi lab[g]
						-10.3	-8.3	0.654	0.012	Bergmann lab
Szalajka	48.1	20.4	9.5	10.1	2.0	-9.9	-8.7	0.664	0.006	Bernasconi lab[g]
Kailas	31.7	82.7	-1.2	15	2.0	1.8	-5.2	0.596	0.006	Eiler lab[b]
Lake Crowley	37.6	-118.7	8.4	18.5	3.0	-1.2	-14.9	0.638	0.019	Eiler lab[d]
Lake Mead	36.3	-114.4	17.7	28.2	3.0	-8.9	-8.9	0.622	0.000	Eiler lab[d]
Mono Lake	37.9	-119.0	8.4	19.4	3.0	6.9	-2.2	0.607	0.002	Eiler lab[d]

Travertines

Aqua Borra*	43.3	11.4	14.4	36.1	2.0	2.3	-8.1	0.565	0.012	Bernasconi lab[g]
						1.7	8.4	0.577	0.011	Bergmann lab
Bagnoli	43.4	11.1	14.8	23.7	2.0	5.5	-7.6	0.591	0.008	Bernasconi lab[g]
BSF Fosso Bianco	42.9	11.7	14.4	44.6	2.0	7.4	-9.9	0.542	0.006	Bernasconi lab[g]
Bük*	47.4	16.8	10.6	54.9	2.0	2.2	-15.1	0.530	0.008	Bernasconi lab[g]
						2.2	-15.0	0.541	0.012	Bergmann lab
Madre del Agua*	28.2	-16.6	-	33.8	2.0	0.2	-10.3	0.566	0.010	Bernasconi lab[g]
						0.1	-10.2	0.584	0.013	Bergmann lab
Igal*	46.5	17.9	10.7	75.0	2.0	0.7	-13.6	0.469	0.007	Bernasconi lab[g]
						0.6	-13.5	0.475	0.011	Bergmann lab
Köröm	48.0	21.0	10.2	79.2	2.0	3.6	-22.0	0.461	0.006	Bernasconi lab[g]
Baishuitai - summer*	27.5	100.0	7.2	12.0	2.0	5.5	-14.3	0.637	0.006	Bernasconi lab[g]
						5.4	-14.3	0.633	0.012	Bergmann lab
Baishuitai - winter*	27.5	100.0	7.2	5.0	2.0	5.2	-12.8	0.637	0.008	Bernasconi lab[g]
						5.1	-12.7	0.635	0.011	Bergmann lab
Piscine Carletti	42.4	12.1	14.5	57.9	2.0	7.3	-12.4	0.511	0.007	Bernasconi lab[g]
Rapolano Terme	43.3	11.6	14.4	28.0	2.0	3.8	-7.5	0.574	0.009	Bernasconi lab[g]
Szèchenyi Spa	47.5	19.1	11.0	70.9	2.0	2.9	-20.5	0.473	0.008	Bernasconi lab[g]
Terme Sangiovanni	43.3	11.6	14.4	41.2	2.0	2.6	-8.9	0.580	0.006	Bernasconi lab[g]
Tura*	47.6	19.6	9.9	95.0	2.0	3.7	-23.3	0.416	0.011	Bernasconi lab[g]
						3.7	-23.2	0.409	0.012	Bergmann lab
Narrow Gauge, Yellowstone*	44.6	-110.4	0.0	60.4	2.0	3.8	-24.5	0.504	0.006	Bernasconi lab[g]

| 3.6 | -24.6 | 0.505 | 0.012 | Bergmann lab |

224

Table 1: Site information and stable and clumped isotope results for freshwater carbonates used in this study. Mean annual air temperatures (MAAT) are averages of the long-term monthly means from each of our sites from 1981-2010, using the University of Delaware's high resolution gridded air temperature dataset (Willmott & Matsuura, 2001) provided by NOAA (https://psl.noaa.gov/data/gridded/data.UDel_AirT_Precip.html). Samples from Eiler Lab at Caltech were processed in the CDES reference frame and projected into I-CDES following the methodology described in Bernasconi et al. (2021).

*Data from the Bernasconi Lab at ETH was recalculated using the methodology described in Bernasconi et al. (2021) and data from the Bergmann Lab at MIT was taken from Anderson et al. (2021).

[a] Recalculated from Wang et al. (2021)

[b] Recalculated from Huntington et al. (2015)

[c] Recalculated from Li et al. (2021)

[d] Recalculated from Huntington et al. (2010)

[e] Recalculated from Petryshyn et al. (2015)

[f] Recalculated from Santi et al. (2020)

[g] Recalculated from Bernasconi et al. (2018)

242   2.2 Sample Preparation

243   2.2.1 Biologic carbonates

244   Aquatic gastropod and bivalve shells were first separated by taxon. Organic material was
245   removed from shells by scraping and sonicating in Milli-Q deionized water until clean. Samples
246   were dried overnight at 50°C, and complete shells were powdered using a mortar and pestle, and
247   reacted with 3% hydrogen peroxide for 60 minutes (Eagle, Eiler, et al., 2013) to remove any
248   remaining organic material. Depending on carbonate content of the gastropod and bivalve shells
249   and instrument sensitivity at the time of analysis, samples were weighed out for mass
250   spectrometric analysis, typically in amounts varying between 5 and 10 mg for a single replicate.

251   2.2.2 Fine grained carbonates

252   Samples of unconsolidated calcareous particles, assumed to be micrite, were
253   disaggregated in Milli-Q deionized water, after which the mixture was poured through a 212 μm
254   steel mesh filter and left to settle in a beaker for 10 minutes. The residue was poured into a
255   second beaker after filtration to remove any remaining suspended material, and this process was
256   repeated until virtually no observable settling occurred. The final residue was treated with 3%
257   hydrogen peroxide for 60 minutes to remove any remaining organic material (Eagle, Eiler, et al.,
258   2013). Resulting micrite was collected on a 0.45 μm cellulose nitrate filter membrane and dried
259   at 50°C. Depending on carbonate content and instrument sensitivity, the amount of sample
260   utilized for mass spectrometry varied between 10 and 30 mg for a single replicate.

261   2.2.3 Biologically mediated carbonates

262   Tufas and microbialites were cut perpendicular to laminae, and polished slabs and thin
263   sections were prepared in order to target specific zones for analysis. Samples were ground into a
264   fine powder using a microdrill. To prevent potential bond reordering due to frictional heating, the
265   drilling during this process was limited in duration and speed (rpm). Samples were reacted with
266   3% hydrogen peroxide for 60 minutes to ensure removal of any organics and dried overnight at
267   50°C (Eagle, Eiler, et al., 2013). Drilled samples were weighed out in 5 to 15 mg aliquots for
268   mass spectrometry depending on the carbonate content of the sample and instrument sensitivity
269   at time of analysis.

270   2.3 Stable Isotope Measurements

271   All samples were run at the University of California, Los Angeles on a Thermo 253 Gas
272   Source isotope ratio mass spectrometer in the Eagle-Tripati Laboratory from 2012-2019,
273   primarily between 2013 and 2015. Methods are described in detail in Upadhyay et al. (2021).
274   Briefly, carbonate samples were first reacted with 105% phosphoric acid for 20 minutes on a
275   90°C online common phosphoric acid bath system, whereby solid carbonate reacts to produce
276   CO_2 gas for analysis. Acid temperature was monitored with a thermocouple throughout each
277   analysis and checked daily for drift. Each sample gas was cryogenically purified using an
278   automated purification system that was modeled on the previously described system at the
279   California Institute of Technology (Passey et al., 2010). The liberated gas from each sample
280   passed through two separate gas traps to ensure the removal of water and other compounds: the
281   first (containing ethanol) is kept at -76°C by dry ice, and the second (containing liquid nitrogen)
282   is kept at -196°C. After sample gas undergoes cryogenic purification, the sample gas is passed

283   through silver wool to remove sulfur compounds (e.g. halocarbons and hydrocarbons; Spencer
284   & Kim, 2015) and remaining trace contaminants were separated by moving the resultant gas
285   through a Thermo Trace GC Ultra gas chromatograph column, which is filled with a divinyl
286   benzene polymer trap, Porapak Q at -20°C (L. M. Santi et al., 2020; Tripati et al., 2015). The
287   purified sample gas was passed on to the mass spectrometer for analysis.

288   Data was collected over nine acquisitions consisting of 10 cycles each to determine $\delta^{13}C$,
289    $\delta^{18}O$, Δ_{47}, Δ_{48}, and Δ_{49}. During each acquisition on the mass spectrometer, sample isotope values
290   were measured relative to high purity Oztech brand CO_2 reference gas ($\delta^{18}O = 25.03‰$
291   VSMOW, $\delta^{13}C = -3.60‰$ VPDB). Equilibrated CO_2 gas standards and carbonate standards were
292   typically run every 3-4 analyses and used for standardization. Averages for our standard values
293   can be found in Supplementary Table 2.

294   2.4 Data handling

295   Table 1 reports isotopic data for samples used within this study. Data processing is
296   detailed in Upadhyay et al., 2021. Data are reported on the I-CDES scale which projects values
297   into a 90°C reference frame. Acid digestion fractionation factors used for calcite and aragonite
298    $\delta^{18}O$ are reported in Swart et al. (1991) and Kim et al. (2007), respectively; for calculations of
299   water $\delta^{18}O$, we use the equations of Kim and O'Neil, (1997) for calcite and Kim et al. (2007), for
300   aragonite. For samples measured in the Eagle-Tripati Lab, raw mass spectrometer data was
301   processed using *Easotope* (Daëron et al., 2016; John & Bowen, 2016). Data is included in the
302   supplement. We excluded replicates if results were consistent with high organic content, as
303   indicated by anomalous Δ_{48} or Δ_{49} for a given correction interval, with samples having values
304   that are more than 3 sigma from the standards being flagged for possible exclusion (Upadhyay et
305   al., 2021). We also exclude replicates with anomalous values of Δ_{47} (I-CDES), $\delta^{13}C$ (VPDB) and
306    $\delta^{18}O$ (VPDB), of more than 3σ from the remaining replicates, which can reflect incomplete
307   digestion or contamination (Tripati et al., 2015). We performed at least three replicate analyses
308   of each sample unless the amount of material available limited the number of analyses; if less
309   than three replicates were run for a sample, we propagated both the internal reproducibility of the
310   sample and the average external reproducibility of the samples in this study to determine the
311   uncertainty of the reported value.

312   Data from published studies (Anderson et al., 2021; Bernasconi et al., 2018; Huntington
313   et al., 2010, 2015; H. Li et al., 2021; Petryshyn et al., 2015; Wang et al., 2021), were reprocessed
314   using current data handling procedures and projected into the I-CDES reference frame, following
315   methods described in Upadhyay et al. (2021) and Bernasconi et al. (2021). Mean sample values
316   are in Table 1, and the replicate level recalculated values can be found in the Supplementary
317   Material. We included modern authigenic carbonate samples from H. Li et al. (2021) that were
318   previously run in the Eagle-Tripati Lab, with identical data processing. For samples and
319   locations described in Li et al. (2021), we propagated the standard error of the regression used to
320   constrain water temperatures and the temperature error reported in the original publication in
321   quadrature to estimate error for lake temperature values. Modern gastropod samples from Wang
322   et al. (2021), which were also run in the Eagle-Tripati Lab, were reprocessed with the Brand
323   parameter set for inclusion in this work. Data from Huntington et al. (2010), Huntington et al.
324   (2015), and Petryshyn et al. (2015) measured in the Eiler Lab at Caltech was reprocessed using
325   Easotope (John & Bowen, 2016), and standard values for these analyses are reported in
326   Supplementary Table 2. Tufas from Kele et al. (2015) run in the Bernasconi Lab at ETH Zürich

327   were previously recalculated with the Brand parameter set by Bernasconi et al. (2018), and
328   additional replicates were recently measured for the calibration in Anderson et al. (2021), thus,
329   we include both sets of measurements on identical samples from both studies. These data
330   presented in Bernasconi et al. (2018) are projected into the I-CDES reference frame using the
331   methodology and new ETH values presented in Bernasconi et al. (2021). Methodology for
332   clumped isotope analysis for these datasets can be found in the publication that initially reported
333   the data. Comparisons to previously published calibration equations are also shown, with data
334   brought into the 90°C reference frame here using AFF values reported in Petersen et al. (2019).

335   2.5 Regression Methodology

336   Recent work has shown that models derived using ordinary least squares (OLS) perform
337   better than their error-in-variables counterparts (e.g. York regression, Deming regression), with
338   higher accuracy and precision for regression parameters, and perform similarly to Bayesian tools
339   for both calibration of clumped isotopes and for temperature reconstruction (Román Palacios et
340   al., 2021). In this study, we evaluate the relationship between Δ_{47} and growth temperature using
341   Ordinary Least Square regression models fit in the lm R function in the stats package (R Core
342   Team, 2022). To evaluate material specificity within our dataset and compare our derived
343   regression parameters to other studies, we utilize an ANCOVA. Specifically, we evaluate
344   pairwise differences in slopes and intercepts between groups of data. We compare our composite
345   calibration along with our material-specific calibrations to four additional studies: a recently
346   published calibration that includes natural and synthetic samples (Anderson et al., 2021), a
347   'universal' calibration created from a synthesis of clumped isotope calibration studies (Petersen
348   et al., 2019), a calibration derived from authigenic lacustrine carbonates (H. Li et al., 2021), and
349   a recalculated travertine calibration (Bernasconi et al., 2018). All data are either in I-CDES or
350   projected to CDES$_{90}$ using AFF values in Petersen et al. (2019).

351   **3 Results and Discussion**

352   3.1 Seasonality of freshwater carbonate formation

353   Carbonates precipitate in many lakes and can form in various freshwater environments
354   with the extent and depth of carbonate deposition determined by seasonal changes in water
355   chemistry, as well as water depth, slope gradient, and circulation within the basin (Gierlowski-
356   Kordesch, 2010; Platt & Wright, 2009). Carbonates that form at the lake margin include ooids,
357   beach rock, shelly accumulations of gastropods and bivalves, microbialites, and tufa, while deep-
358   water deposits are comprised largely of carbonate muds and grains (such as ostracods) that
359   accumulate below the storm wave base (Platt & Wright, 2009). In most cases, carbonate
360   accumulation is controlled by seasonal changes in saturation (Anadón et al., 2009; Hren &
361   Sheldon, 2012; Kelts & Hsü, 1978; Street-Perrott & Harrison, 2013).

362   Therefore, we aim to use data for samples within our study to evaluate the accuracy of
363   reconstructing the seasonality of formation for different carbonate types. We use the recently-
364   derived calibration from Anderson et al. (2021) that uses a combination of both synthetic and
365   field-collected samples to estimate formation temperature (in this case, lake water temperature
366   for lacustrine samples) using the clumped isotope results presented in this study. These estimates
367   were then compared to predicted values of lake water temperatures for each location using the
368   seasonal lake surface water temperature to mean annual air temperature (MAAT) transfer
369   functions from Hren and Sheldon (2012) and warmest month lake surface water-to-air transfer

370 function from Mering (2015). Riverine and spring samples were excluded from this analysis.
371 MAAT estimates used within these transfer functions are averages of the long-term monthly
372 means from each of our sites from 1981-2010, using the University of Delaware's high
373 resolution gridded air temperature dataset (Willmott & Matsuura, 2001) provided by NOAA. The
374 analysis described below suggests that application of the calibration published by Anderson et al.
375 (2021) to modern freshwater carbonates can, in some cases, yield inaccurate temperatures, given
376 what is known about the seasonality of growth for different carbonate types.

377   Figure 2a shows our derived estimates of seasonal lake temperature using the
378 methodology described above for biogenic carbonates. Biogenic taxa precipitate the majority of
379 shell material during a well-defined "growing" season, typically initiating shell calcification
380 during the spring, as long as food availability and water temperature exceed a species-specific
381 threshold value (Gierlowski-Kordesch, 2010; Hren & Sheldon, 2012; Platt & Wright, 2009;
382 Versteegh et al., 2010; Wilbur & Watabe, 1963). Prior research has shown that in the Northern
383 Hemisphere, the April-October interval has been shown to encompass a majority of shell growth
384 for freshwater mollusks (Apolinarska et al., 2015; Versteegh et al., 2010). However, most
385 individual species have a restricted range of water temperatures that they can tolerate and that
386 allows shell formation, thus, it is likely that calcification occurs within a narrower interval
387 sometime between spring and early summer, when water temperatures fall within the species-
388 specific temperature range (Hren & Sheldon, 2012; Versteegh et al., 2010).

389   When applying the calibration of Anderson et al. (2021), our Δ_{47}-derived temperatures
390 suggest that 37% of our biogenic samples reflect only warmest month water temperatures,
391 implying a relatively narrow window of precipitation for shell precipitation (Fig. 2A). Although
392 water temperature is the primary factor that controls carbonate growth in biotic carbonates, shell
393 formation can be influenced by other environmental factors, such as food availability and
394 primary productivity (Dunca & Mutvei, 2001). Therefore, utilizing a calibration based on both
395 synthetic and natural samples may not capture the appropriate seasonality for freshwater
396 mollusks. Specifically, the Anderson et al. (2021) calibration, when applied to biogenic taxa such
397 as gastropods, may overestimate the water temperature in which the organisms formed,
398 particularly at higher latitudes.

399   Temperature reconstructions from endogenic carbonate precipitation are typically biased
400 towards the warmest period of the year, when carbonate precipitation is enhanced due to
401 evaporation increasing carbonate saturation and photosynthetic uptake lowering pCO$_2$, thereby
402 increasing water pH (Hren & Sheldon, 2012; Oviatt et al., 1994; Platt & Wright, 2009). In the
403 subtropical and polar Northern Hemisphere this corresponds to June – August, while tropical
404 lakes have less variability in lake temperature resulting from decreased seasonality. Although
405 tropical lakes experience decreased seasonality, seasonal changes in rainfall and evaporation
406 within tropical lakes can also play a role in influencing carbonate saturation state.

407   The Δ_{47}-temperature calculated using Anderson et al. (2021) for lower latitude micrite
408 samples imply that early Spring (April - June) is the dominant interval for carbonate precipitation
409 for 35% of the samples, instead of intervals of the most elevated temperatures (Fig. 2b).
410 Estimated temperatures for higher latitudes shows carbonate precipitation mainly occurs during
411 the estimated warmest month, and in some occasions Δ_{47}-temperatures exceed the mean warmest
412 month water temperature value. This could imply that precipitation of endogenic carbonate may
413 be elevated in these settings during short intervals of intense heat and evaporation or indicate that
414 the calibration of Anderson et al. (2021) does not work perfectly for all freshwater carbonates. In

415 total, these observations indicate that the calibration of Anderson et al. (2021) yields
416 temperatures that are broadly consistent with known freshwater carbonate growth seasons and
417 systematics within mid-to-high latitudes, but underestimates lake water temperature in some
418 cases and may not reflect what is known about season of growth in approximately half of the
419 lakes examined here.

420 Biologically-mediated carbonates, including tufas and microbialites, precipitate as a
421 result of local changes in water conditions and biological productivity (Capezzuoli et al., 2014).
422 These carbonates are formed by both abiogenic and biogenic processes, with algae and other
423 aquatic plants influencing their precipitation on organic and inorganic substrates (Capezzuoli et
424 al., 2014; Flügel, 2004). Microbial activity within carbonates can increase rates of
425 photosynthesis, thereby lowering pCO$_2$ and increasing carbonate saturation state making
426 carbonate mineral precipitation more favorable (Pacton et al., 2015; Platt & Wright, 2009; Solari
427 et al., 2010). Additionally, microbial biomass provides a negatively charged surface to which
428 ions may adhere, which locally increases calcium concentration and promotes the supersaturation
429 of carbonates (Fein, 2017). These conditions are enhanced during the warmest interval of the
430 year, when evaporation also plays a role in increasing carbonate saturation, eventually inducing
431 precipitation of shoreline carbonates. Recent field studies of modern tufas and microbialites have
432 shown elevated growth rates during warmer water temperature conditions (Brady et al., 2014;
433 Marić et al., 2020; Pedley, 1990).

434 Reconstructions of water temperature from biologically-mediated carbonates from this
435 study derived using the calibration of Anderson et al. (2021) (Figure 2c) seem to exceed
436 predictions, with four samples matching or exceeding warmest month water temperatures. Prior
437 work analyzing Δ_{47} in modern tufas in Japan has shown that tufas are able to discern seasonal
438 changes in water temperature (Kato et al., 2019). Given that these carbonates are continuously
439 calcifying (although precipitation amount is dependent on season), it is unlikely that precipitation
440 solely occurred during the warmest water temperature intervals and that Δ_{47}-derived
441 temperatures should be reflecting a maximum. Therefore, the application of the Anderson et al.
442 (2021) calibration does not appear to be capturing temperature variability that is contained within
443 biologically-mediated carbonates.

444 Our analysis, on first order, shows that the lake water temperatures derived using the
445 Anderson et al. (2021) calibration often results in unrealistic temperatures for carbonate
446 precipitation for different types of freshwater carbonates. Our results show that the calibration of
447 Anderson et al. (2021), which is dominated by synthetic precipitates and marine carbonates
448 rather than natural samples, may over or underestimate a reasonable temperature range of
449 carbonate formation and may not be ideal for terrestrial paleotemperature reconstructions for all
450 freshwater carbonates. We note that the transfer function-based approach we used (Hren &
451 Sheldon, 2012) does not, for lacustrine carbonates, take into account the size and setting of the
452 water body and potential influences from snowmelt, both of which would impact the difference
453 in temperatures between lake water and overlying air. Thus, in the next section, we derive
454 calibrations that take these factors into account and are specific to different types of terrestrial
455 freshwater carbonates.

a. Biologic carbonates
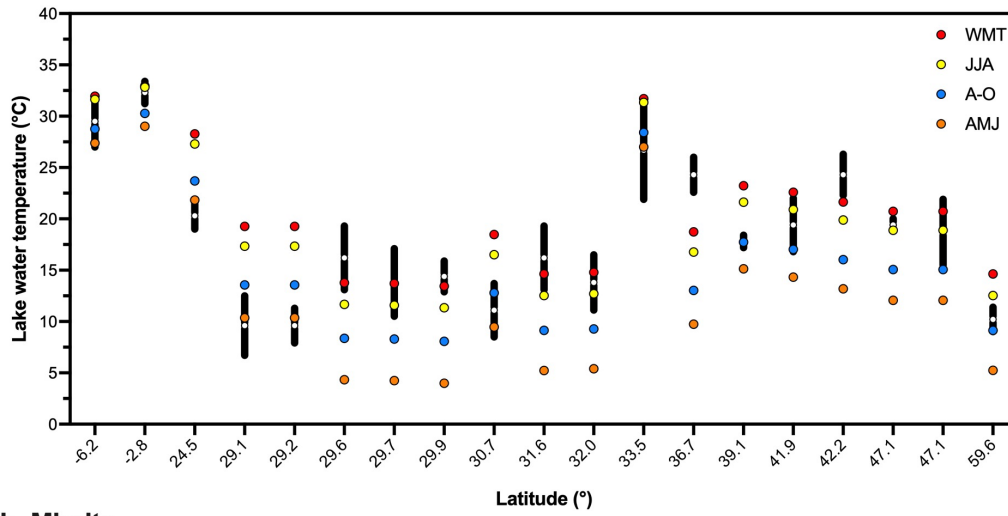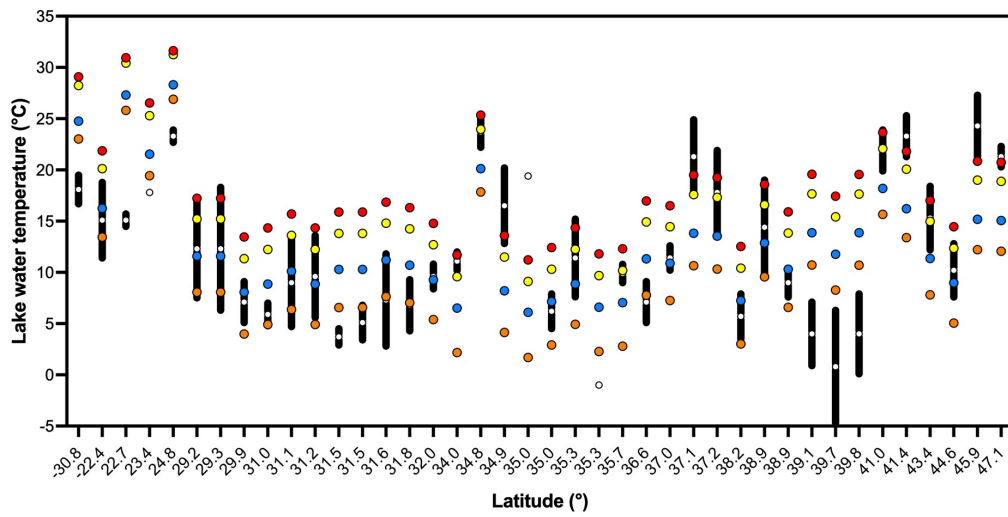
b. Micrite

c. Biologically-mediated carbonates


456
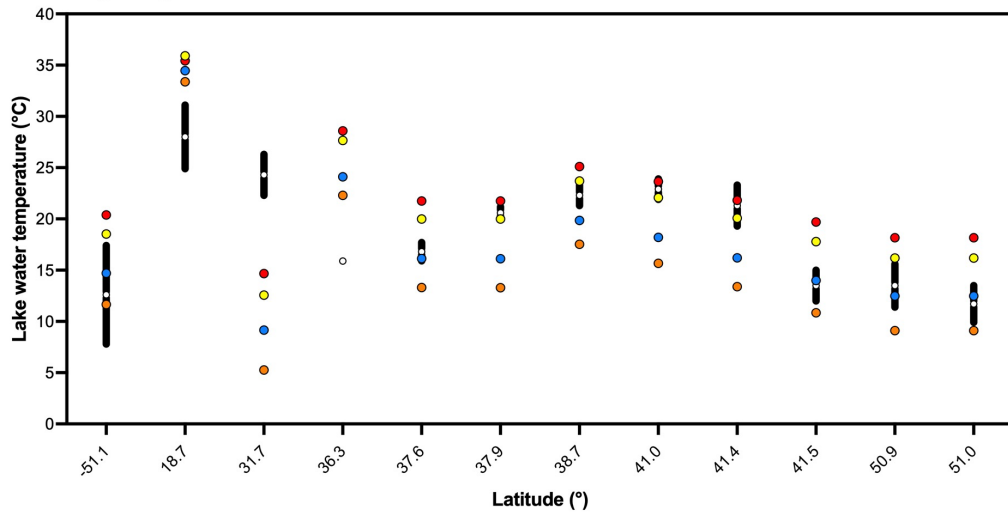
457 **Figure 2: Evaluation of seasonality of carbonate precipitation for biogenic, micrite, and**
458 **biologically mediated lacustrine carbonates using the clumped isotope calibration of**
459 **Anderson et al. (2021).** White circles with black bars are Δ_{47}-derived temperatures and with
460 uncertainties, respectively. Results are compared to projected lake temperatures for different
461 times of year, calculated using relationships from (Hren & Sheldon, 2012) and Mering (2015) in
462 conjunction with MAAT for each location derived from the University of Delaware's high-
463 resolution gridded air temperature dataset (Willmott & Matsuura, 2001) provided by NOAA.
464 Orange circles reflect early spring (Northern Hemisphere April-June (AMJ)) water temperatures,
465 yellow circles indicate summer (Northern Hemisphere June-August (JJA)), blue circles indicate
466 April-October water temperatures (A-O), and red circles indicate warmest month water
467 temperatures (WMT). This comparison shows that for biologic carbonates, there is good
468 agreement between Δ_{47}-T and what is known about typical growth seasons in the Anderson et al.
469 (2021) calibration in lower latitudes. However, the Anderson et al. (2021) calibration results in
470 an overestimation of growth temperature at higher latitudes, with 37% of clumped isotope
471 derived temperatures matching or exceeding estimated lake warmest month temperature, as
472 indicated by the offset between the clumped isotope derived temperatures represented by a white
473 circle with black error bands and the colored data points in panel A. For micrites, the Δ_{47}
474 temperatures derived from the Anderson et al. (2021) calibration are likely underestimated in
475 roughly half of the lakes examined here. Estimated temperatures from biologically mediated
476 carbonates using the Anderson et al. (2021) calibration are reflecting warmest month
477 temperatures in many cases, an overestimation from the projections derived from Hren and
478 Sheldon (2012).

479   3.2 Δ_{47}-Temperature Relationships

480   We utilize calibration data in Table 1 to derive regressions for our entire dataset (a
481 composite freshwater calibration), and material-specific calibrations for biogenic carbonates
482 (bivalves and gastropods), biologically mediated carbonates (microbialites and tufas), micrite,
483 and travertines. Δ_{47} values for samples within this study range from 0.409 to 0.682‰ with
484 independently measured water temperatures ranging from 5 to 95°C. Calibrations derived in this
485 study are presented in Table 2.

486   Performing an ordinary least squares regression through all freshwater carbonate data in
487 this study results in a steeper slope and shallower intercept than Anderson et al. (2021)
488 calibration. Although the 95% confidence intervals on the estimated regression models overlap
489 visually (Fig. 3), an analysis of covariance (ANCOVA) analysis shows that the slopes for the
490 two calibrations are significantly different from each other (p_{slope} = 0.0334; Table 3). The
491 Anderson et al. (2021) calibration includes low temperature Antarctic microbialites that are
492 offset from other data, with half of the samples from a high pH (10.3-10.7; Mackey et al., 2017)
493 environment (Fig. 3 - dark red symbols). Low temperature and high pH are environmental
494 factors that could give rise to potential kinetic isotope effects or DIC speciation effects (Tang et
495 al., 2014; Tripati et al., 2015). In fact, all of the Antarctic samples are negatively offset from the
496 rest of the data in this study, and thus, we exclude these data from both the composite and the
497 biologically-mediated regressions we report in this study (Table 3). Additionally, we compare
498 our results from the composite calibration to the synthesis of calibration data published in
499 Petersen et al. (2019) that was projected into a 90°C reference frame. Similarly to Anderson et al.
500 (2021), we find that the slope derived within this study yields a statistically significant difference
501 in slope to that of Petersen et al. (2019) (p_{slope} = 0.0036; Table 3). Despite improvements in data
502 handling and standardization procedures that have been shown to resolve disparities in derived
503 regression slopes in two large synthesis studies (Anderson et al., 2021; Petersen et al., 2019), we
504 do not observe convergence between regression parameters derived from these syntheses and our
505 composite freshwater regression (Fig. 3). However, our derived freshwater composite calibration
506 parameters show agreement with two previous calibrations using authigenic lacustrine
507 carbonates (H. Li et al., 2021) and travertines (Bernasconi et al., 2018) (Table 3).

$$\Delta_{47} = (0.0420 \pm 0.0013) \times 10^6/T^2 + (0.1270 \pm 0.0152)$$
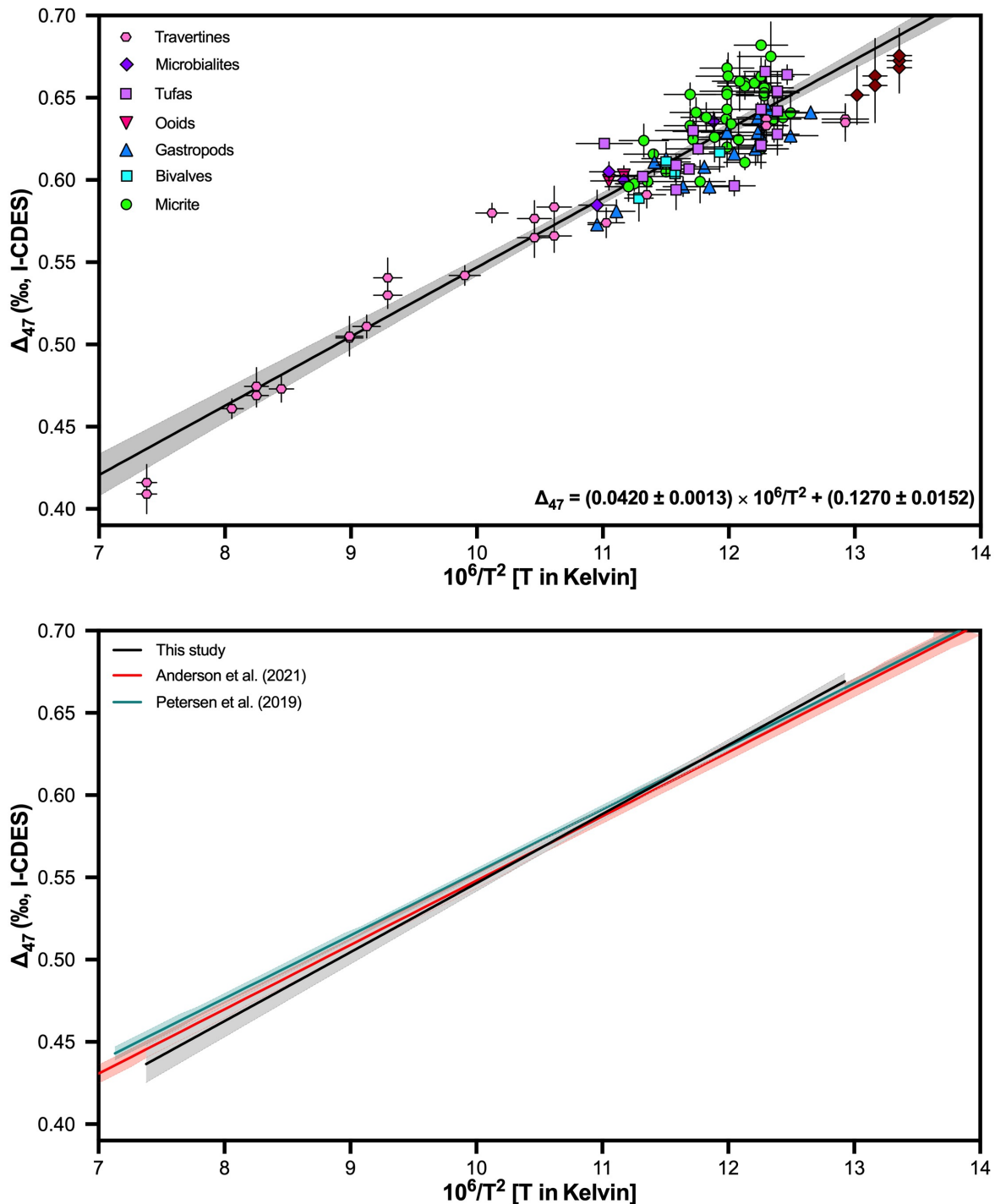
508
509 **Figure 3: Top: Δ_{47}-temperature relationship for all 108 freshwater carbonates included in**
510 **this study.** Black line represents a linear, ordinary least squares regression through the data and
511 the gray shaded area represents the 95% confidence interval. We find a strong relationship
512 between Δ_{47} and temperature($p < 0.0001$; $r^2 = 0.8959$). Red diamonds represent low temperature
513 and/or high pH lacustrine microbialites from Anderson et al. (2021) that have been excluded
514 from the regression. **Bottom: Comparison of our composite freshwater regression to**

515   **previously published clumped isotope calibrations.** ANCOVA results show that the slope
516   derived for our calibration is statistically different from the acid corrected calibration of Petersen
517   et al. (2019) and Anderson et al. (2021), with p_{slope} values of 0.0036 and 0.0334, respectively
518   (Table 3). Our calibration yields higher temperature estimates than Anderson et al. (2021) in the
519   range of natural carbonate growth, but similar temperatures to Petersen et al. (2019)
520   (Supplementary Table 3).

	n	Slope			Intercept			r²	p
Composite	108	0.0420	±	0.0013	0.1270	±	0.0152	0.9053	<0.0001
Biologic	23	0.0371	±	0.0043	0.1739	±	0.0510	0.7811	<0.0001
Micrite	38	0.0462	±	0.0074	0.0844	±	0.0890	0.5170	<0.0001
Bio-mediated	22	0.0345	±	0.0067	0.2164	±	0.0798	0.5669	<0.0001
Travertine	23	0.0398	±	0.0020	0.1450	±	0.0203	0.9487	<0.0001

521 **Table 2: Derived regression parameters for all freshwater calibration data and material**
522 **specific calibration data using linear, ordinary least squares regression.**

Regression parameter: slope

	This study: composite	This study: biologic	This study: micrite	This study: bio-mediated	This study: travertine	Bernasconi et al. (2018)a: travertine	Li et al. (2020)b: micrite	Petersen et al. (2019)b	Anderson et al. (2021)
This study: composite	—	—	—	—	—	0.8620	0.3080	0.0036	0.0334
This study: biologic	—	—	0.4880	0.7463	0.6730	0.3217	0.1181	0.9456	0.7660
This study: micrite	—	0.4880	—	0.3785	0.6114	0.8474	0.5534	0.4590	0.4880
This study: bio-mediated	—	0.7463	0.3785	—	0.4580	0.2110	0.1040	0.6770	0.4852
This study: travertine	—	0.6730	0.6114	0.4580	—	0.2810	0.1650	0.3620	0.6320
Bernasconi et al. (2018)a: travertine	0.8620	0.3217	0.8474	0.2110	0.2810	—	0.2530	0.0260	0.0363
Li et al. (2020)b: micrite	0.7100	0.3679	0.5534	0.3190	0.5240	0.6970	—	0.4480	0.4163
Petersen et al. (2019)b	0.0036	0.9456	0.4590	0.6770	0.3620	0.0260	0.1430	—	0.2078
Anderson et al. (2021)	0.0334	0.7660	0.4880	0.4852	0.6320	0.0363	0.0953	0.2078	—

Regression parameter: intercept

	This study: composite	This study: biologic	This study: micrite	This study: bio-mediated	This study: travertine	Bernasconi et al. (2018)a: travertine	Li et al. (2020)b: micrite	Petersen et al. (2019)b	Anderson et al. (2021)
This study: composite	—	—	—	—	—	0.6510	0.2850	—	—
This study: biologic	—	—	0.0000	0.0047	0.6320	0.0082	0.0215	0.0728	0.2710
This study: micrite	—	0.0000	—	0.0379	0.0050	0.0264	0.0014	0.0000	0.0000
This study: bio-mediated	—	0.0047	0.0379	—	0.1140	0.6580	0.4100	0.2540	0.0542
This study: travertine	—	0.6320	0.0050	0.1140	—	0.4570	0.4550	0.0354	0.4440
Bernasconi et al. (2018)a: travertine	0.6510	0.0082	0.0264	0.6580	0.4570	—	0.5110	—	—
Li et al. (2020)b: micrite	0.2850	0.0215	0.0014	0.4100	0.4550	0.5110	—	0.6800	0.2290
Petersen et al. (2019)b	—	0.0728	0.0000	0.2540	0.0354	—	0.6800	—	0.0835
Anderson et al. (2021)	—	0.2710	0.0000	0.0542	0.4440	—	0.2290	0.0835	—

523

Table 3: **Results of the ANCOVA test for calibration-pairs for slope and intercept.** Red shading indicates differences in parameters with 95% confidence ($p < 0.05$), yellow shading indicates differences in parameters with 90% confidence ($0.05 < p < 0.10$), and green shading indicates no statistically significant difference between parameters. Top: ANCOVA results for slope. 27 pairs have a p value > 0.1, demonstrating a convergence of slope when looking at material-specific groups of data. Bottom: Results of the ANCOVA test for calibration-pairs for intercept. This analysis is only performed on calibration pairs that had p-values exceeding 0.1 for the slope analysis. Differences in intercepts between different groups of data in this study were prevalent in 4 pairwise comparisons ($p < 0.05$), thus, material specific calibrations may be appropriate for climate reconstructions. *Δ_{47} values were corrected to a 90°C reference frame using AFF presented in Petersen et al. (2019). **Δ_{47} values were corrected to I-CDES using Equation A.7. in Bernasconi et al. (2021).

536 **3.2.1 Evidence for material-specificity in regression models**

537   Given the finding that the calibration slope of Anderson et al. (2021) does not statistically
538 match the larger composite calibration of freshwater carbonates assembled here (Figure 3; Table
539 3) and also does not fit well with data from freshwater carbonates from certain latitudes and
540 environments (Figure 2), we proceed by testing the hypothesis that there could be material-
541 specific calibrations. We derive calibrations for biologic carbonates (bivalves and gastropods),
542 biologically-mediated carbonates (microbialites and tufas), micrites, and travertines, and test
543 whether regression parameters differed between these groups of materials (Table 2; Figure 3).

544   3.2.1.1 Biogenic Carbonates

545   Our biogenic carbonate calibration was developed using 137 analyses from 23 samples
546 with Δ_{47} values and independently constrained water temperatures ranging from 0.573-0.643‰
547 and 7 - 29°C, respectively. This dataset includes 16 new samples, alongside reprocessed data
548 from Huntington et al. (2015) and Wang et al. (2021) that have been brought onto the I-CDES
549 reference frame. Our calibration shows a significant temperature dependence (Figure 4a; p =
550 <0.0001) between the clumped isotope signal and temperature and samples demonstrate
551 agreement with our linear model (r^2 = 0.7811).

552   Our results show that biogenic carbonates record more depleted Δ_{47} values relative to
553 other freshwater samples in this study (Fig. 3) and the resulting calibration line has a lower
554 intercept relative to the Petersen and Anderson calibrations (Figure 4A). Despite visually
555 appearing to be offset from the rest of the data (Figure 3), we find no statistical difference in
556 slopes between our Δ_{47}-T regression of biogenic carbonates and other carbonate groups within
557 this study (Table 3). However, an ANCOVA analysis finds significant differences in intercepts
558 between biogenic carbonates and micrite ($p_{intercept}$ = <0.0001) and biologically mediated
559 carbonates ($p_{intercept}$ = 0.0047) (Table 3). When comparing our calibration results to the
560 calibrations presented in Anderson et al. (2021), H. Li et al (2021), Bernasconi et al. (2018), and
561 Petersen et al. (2019), our ANCOVA indicates shows no difference in slope between our
562 biogenic carbonate calibration, but differences in intercept between our study and the authigenic
563 carbonate calibration presented in H. Li et al. (2021) ($p_{intercept}$ = 0.0215) and the 'universal'
564 calibration derived by Petersen et al. (2019) ($p_{intercept}$ = 0.0728) (Table 3). We find no differences
565 in either slope or intercept between biogenic carbonates and the recent I-CDES calibration of
566 Anderson et al. (2021)

567   The depletion in Δ_{47} observed within these biologic samples relative to micrites,
568 travertines, tufas, and microbialites could stem from changes in growth rate as a function of
569 season, or other unidentified factors. As the sample size requirements for clumped isotopes is
570 relatively large, it often requires the analyses of a complete shell or the majority of a shell for
571 analyses, effectively integrating seasonal signals recorded in the shell and potentially leading to a
572 more muted temperature sensitivity of the calibration than if seasonally resolved sampling could
573 be carried out. Additionally, there is potential for a mismatch of temperature between in-situ
574 measured temperatures, which is representatitve of a multi-year average, and the temperature
575 range experienced by biologic samples considering that the lifespan when shell growth would
576 occur is limited to a mush shorter timeframe. Another possibility is that kinetic isotope
577 fractionations may manifest in freshwater gastropod and bivalve shells, as have been constrained
578 in other biocarbonates such as coral skeletons (Ghosh, Adkins, et al., 2006; Saenger et al., 2012).
579 However, more research is needed to draw this conclusion for freshwater biologic carbonates

580   including potentially performing culturing experiments at controlled temperatures as well as
581   examining other geochemical indicators such as Δ_{48} measurements. We note that although in-
582   depth study of clumped isotope fractionations in aquatic freshwater gastropods is limited to this
583   study, work with modern land snails has shown that a majority of these samples also are offset to
584   lighter Δ_{47} values than the Petersen et al. (2019) calibration (Dong et al., 2021). Culture
585   experiments on species of freshwater gastropods and bivalves may help to better constrain the
586   origin and impact of these effects.

587   3.2.1.2 Micrites

588   In our study we present 2 new samples of micrite, and reprocess data from 33 samples
589   from Li et al. (2021) and 3 samples from Huntington et al. (2010) to be on the I-CDES reference
590   frame. Micrites in this study include water temperatures between 9.8 and 29.0°C and Δ_{47} values
591   from 0.596 to 0.682‰. Micrites evaluated in this study demonstrate a significant temperature
592   dependence (p<0.0001; Figure 4b), however, our samples demonstrate significant variability (r^2
593   = 0.5736).

594   Comparing our derived micrite parameters to other carbonate groups in this study, we
595   find no significant difference in slopes between materials, but find significant differences in
596   intercept between micrites and biogenic carbonates ($p_{intercept}$ = <0.0001), biologically mediated
597   carbonates ($p_{intercept}$ = 0.0379), and travertines ($p_{intercept}$ = 0.0050). Visually, we find that the
598   micrite regression is positively offset relative to both the Anderson et al. (2021) and Petersen et
599   al. (2019) calibrations (Figure 4b). In contrast to the agreements in slope, our ANCOVA analysis
600   finds significant differences in intercept between a published travertine calibration (Bernasconi
601   et al., 2018; $p_{intercept}$ = 0.0264), an authigenic carbonate calibration (H. Li et al., 2021; $p_{intercept}$ =
602   0.0014), a large calibration dataset (Petersen et al., 2019; $p_{intercept}$ = <0.0001), and a recently
603   published calibration on the I-CDES scale (Anderson et al., 2021; $p_{intercept}$ = <0.0001).

604   Prior work analyzing clumped isotope composition suggests that Δ_{47} values of authigenic
605   carbonates precipitate near equilibrium, and are not impacted by disequilibrium fractionations
606   related to carbonate precipitation rate or water chemistry (H. Li et al., 2020). Thus, the variability
607   in Δ_{47} that we observe for micrite is potentially due to uncertainty in the timing of surface
608   carbonate precipitation events at each site. Micrite precipitation is enhanced by biological
609   processes such as algal blooms and temperature effects which can peak at different times
610   throughout the year, and behavior of precipitation events varies depending on characteristics of
611   the lake (i.e. open or closed; location; stratification/ventilation; etc.)(Hren & Sheldon, 2012).
612   Additionally, we note that the samples from UCLA were sieved through 212 μm mesh, which
613   may include juvenile or fragments of mature ostracodes, and it is unclear if any screening for
614   additional fossil material occurred for samples first published in Huntington et al. (2010) was
615   performed. However, the majority of the samples recalculated in this synthesis from H. Li et al.
616   (2021) were filtered through a 45 μm mesh and screened for ostracode valves. Ostracode valves
617   in the sediment may bias temperature estimates derived by clumped isotope analysis, given that
618   different factors control organism growth, thus, the inclusion of potential fragments of fossilized
619   material may be a source of the increased scatter we see in the Δ_{47}-temperature dependence for
620   micrites.

621   3.2.1.3 Biologically Mediated Carbonate

622   The calibration for biologically mediated carbonates is constructed with 255 analyses of
623   24 samples, including 7 new samples, 13 reprocessed samples from Santi et al. (2020), Petryshyn
624   et al. (2015), Huntington et al. (2015), Huntington et al. (2010), and Bernasconi et al. (2018) that
625   were converted into I-CDES, and 4 samples taken from Anderson et al. (2021). Water
626   temperatures for biologically mediated samples span 18.9°C (10.1 - 29.0°C) and Δ_{47} values range
627   between 0.585-0.666‰. We find significant variability in our dataset (Figure 4c; $r^2 = 0.5669$)
628   and a significant relationship between Δ_{47} and temperature (p = <0.0001).

629   Although we do not see statistically significant differences in slopes between
630   biologically-mediated carbonates and other freshwater carbonate types, an ANCOVA detects
631   differences in intercept between biologically mediated carbonates and biogenic carbonates
632   ($p_{intercept} = 0.0047$) and micrite ($p_{intercept} = 0.0379$). We also find significant differences in
633   intercept between the biologically mediated regression and the I-CDES calibration of Anderson
634   et al. (2021) ($p_{intercept} = <0.0001$).

635   Overall, the biologically-mediated regression results in warmer temperature predictions,
636   in particular at higher temperatures, relative to biogenic carbonates and travertines analyzed in
637   this study as well as the Anderson calibration (Table 2; Supplemental Table 3), suggesting that
638   biologic processes may influence observed Δ_{47}-temperature relationships (also could be a source
639   of scatter; $r^2 = 0.5669$). Similar discrepancies between tufa and synthetic samples were observed
640   in Kato et al. (2019), who reported values from tufa samples predicted by synthetic calibrations
641   that were higher than modern environmental temperatures. However, the modern tufa data from
642   Kato et al. (2019) is not included in this synthesis due to discrepancies between standard values
643   for Carrara Marble and NBS-19 relative to what was reported by Bernasconi et al. (2021) and
644   Uphadhyay et al. (2021), although we note their calibration falls within our 95% confidence
645   interval of our biologically-mediated calibration.

646   3.2.1.4 Travertines

647   Although we did not add new data, we created a regression for travertine samples
648   containing 543 analyses from 23 samples. The travertine dataset includes data from 15
649   recalculated samples from previous publications to be on the I-CDES reference frame
650   (Bernasconi et al., 2018; Kele et al., 2015) following methodology in Bernsconi et al. (2021) and
651   8 new published measurements (Anderson et al., 2021), to analyze them within the same
652   statistical framework used here. Travertine samples encompass the largest range of
653   independently measured water temperatures (5 - 95°C) and Δ_{47} values (0.409-0.637‰). Similarly
654   to the other groups of carbonate considered in this study, we find a significant temperature
655   dependence (slope; p = <0.0001) and a high degree of agreement between the fitted values and
656   calibration data points ($r^2 = 0.9487$). Travertines display the highest r^2 values relative to biogenic
657   carbonates, biologically mediated carbonates, and micrites, which may arise if they have the least
658   complex precipitation mechanism with little biological influence relative to the other groups.

659   ANCOVA tests indicate the travertine linear regression did not have a statistically
660   significant slope compared to other groups of freshwater carbonates in this study, but does
661   indicate a statistically different intercept to the micrite regression ($p_{intercept} = 0.0050$; Table 3).
662   The newly-derived regression on the updated I-CDES reference frame is statistically
663   indistinguishable from the previous travertine calibration presented in Bernasconi et al. (2018),

664   but has significant differences in intercept from the calibration presented in Petersen et al. (2019)
665   ($p_{intercept}$ = 0.0354), suggesting that applying a 'universal' calibration may not be appropriate.
666   Additionally, we find no significant differences in either slope or intercept between travertines
667   and the Anderson et al. (2021) calibration or authigenic lacustrine carbonate calibration of H. Li
668   et al. (2021) (Table 3).

669   3.2.1.5 Comparison of material-specific and composite calibrations

670   Overall, we observe no statistically significant difference between the calibration slopes
671   derived from different materials and previously published calibrations (Table 3) when freshwater
672   carbonates are divided into groups to account for differences in their precipitation (e.g.
673   seasonality, ecology, etc.), calibrations converge on a common temperature dependence (slope)
674   for clumped isotope measurements. A similar convergence of slopes was found in Petersen et al.
675   (2019) when comparing 14 different clumped isotope studies of both biogenic and abiogenic
676   carbonates using updated parameter values for Δ_{47} calculation. Anderson et al. (2021) also found
677   a convergence of slopes between their new data, the Petersen calibration, and recalculated
678   calibration lines using updated carbonate standardization procedures for 4 recent calibration
679   studies. However, our ANCOVA analyses also indicate statistically different intercepts for most
680   of our calibrations from groups of freshwater carbonates (Table 3). Our findings are unchanged
681   if we only consider samples that were analyzed at UCLA.

682   In order to evaluate goodness of fit between the two types of models presented in this
683   study, we use root mean square error (RMSE) to evaluate the differences between our directly
684   measured and Δ_{47}-derived measurements. Applying our composite calibration to biogenic
685   samples results in a RMSE of 4.4°C, while applying the biogenic calibration results in a RMSE
686   of 2.9°C, showing a better fit when using the material-specific calibration. Temperatures derived
687   from a micrite-specific calibration results in a lower RMSE than a composite calibration (3.9°C
688   and 4.6°C, respectively). Contrastingly, the composite calibration outperforms the material
689   specific calibrations for biologically mediated carbonates and travertines, resulting in a lower
690   RMSE than their material specific counterparts (tufa: 4.4°C and 5.1°C, travertine: 6.5°C and
691   7.1°C). Figure 5 shows the impact of the applied calibration on temperature reconstructions
692   using both the composite and material specific calibrations derived in this study, showing a
693   decrease in residuals when utilizing material-specific regressions for all material types. Thus, it
694   may be more appropriate to use material-specific calibrations when reconstructing
695   paleotemperatures. However, we also note that the application of material-specific calibrations
696   will necessitate using fewer data points (minimum n = 22) over a more limited temperature range
697   in most cases (except for travertines), both factors of which could increase uncertainty in the
698   calibration. We recommend using material specific calibrations for samples that fall within the
699   original observation range, given that application of material specific calibrations to samples
700   from more extreme temperatures could necessitate calibration extrapolation.

a. Biologic carbonates
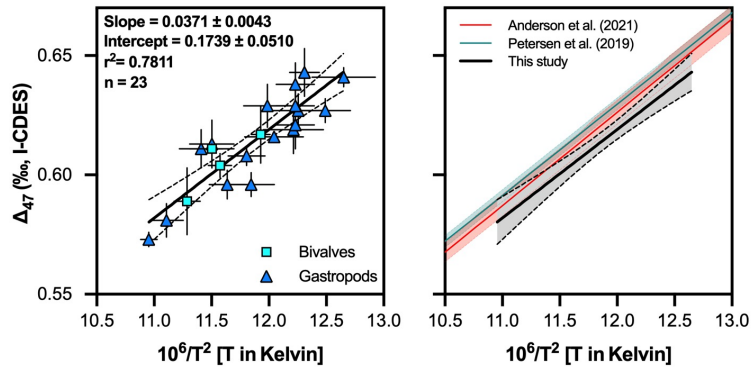

b. Micrite
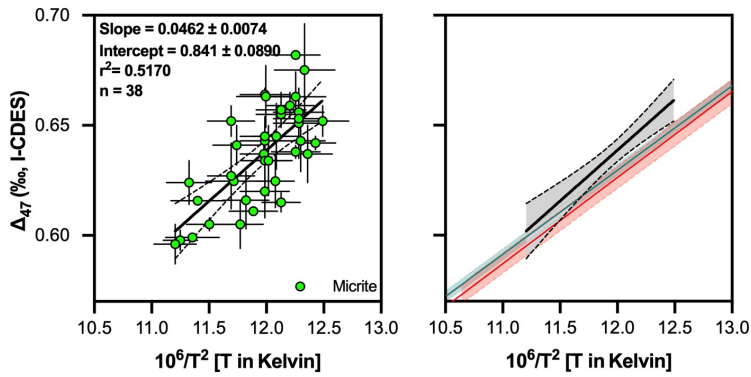
c. Biologically-mediated carbonates

d. Travertines

701
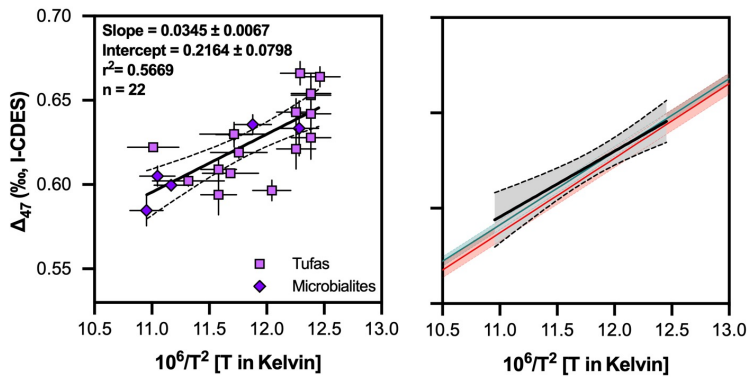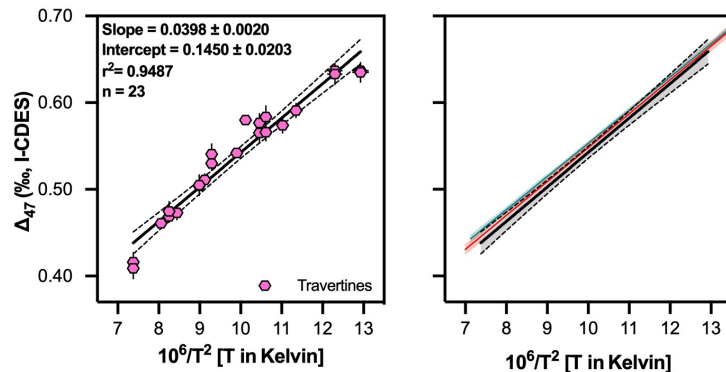
702   **Figure 4: Δ₄₇-temperature relationships for different groups of freshwater carbonates.** Left:
703   Δ_{47}-temperature relationship for all carbonate types included in this study. Black line represents a
704   linear, ordinary least squares regression through the data. We find a strong relationship between
705   Δ_{47} and temperature for each group of data. We find indistinguishable slopes between all groups
706   of data, but find statistically different intercepts between a majority of datasets (Table 3),
707   suggesting that material-specific calibrations may be most appropriate. Right: Derived
708   comparison of our material-specific calibrations to previously published clumped isotope
709   calibrations. We find statistically similar slopes between all of our material-specific regressions
710   and the slopes presented in Petersen et al. (2019) and Anderson et al. (2021), showing a
711   convergence of slope (temperature dependence) throughout the studies. However, we find
712   significant differences in intercept between previously published work and most of our derived
713   calibrations (Table 3), indicating these calibrations are systematically offset from each other.

a. Water temperature
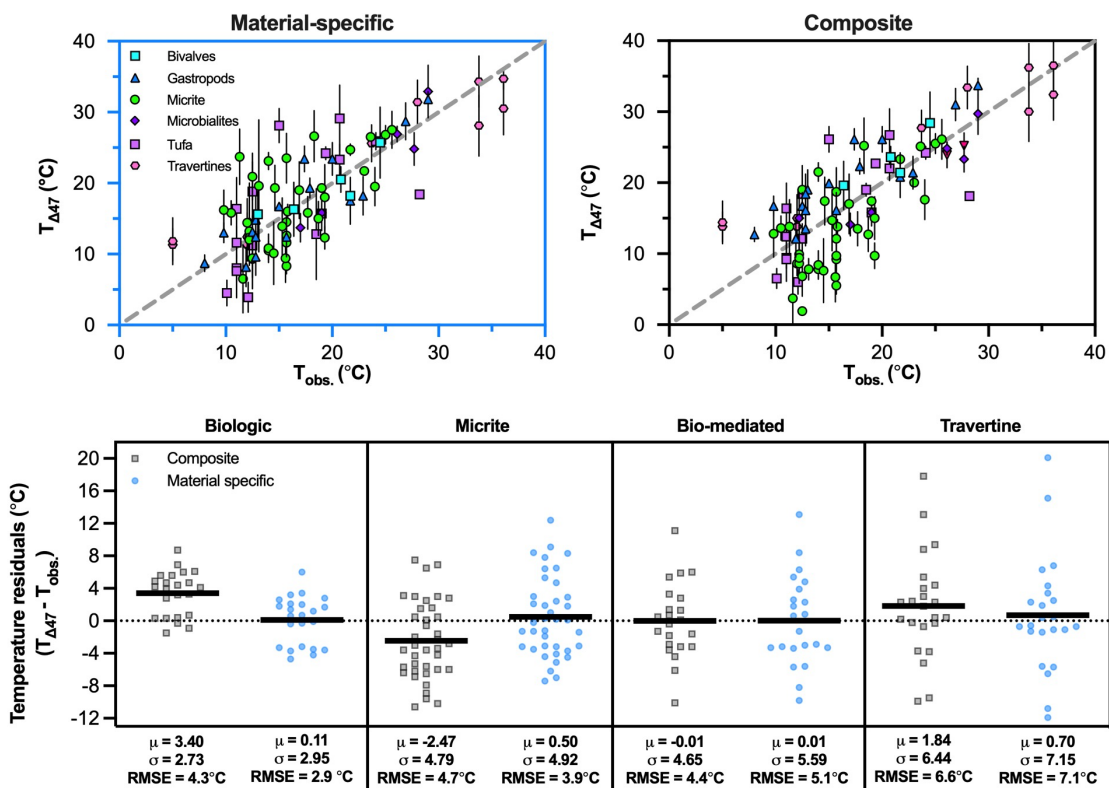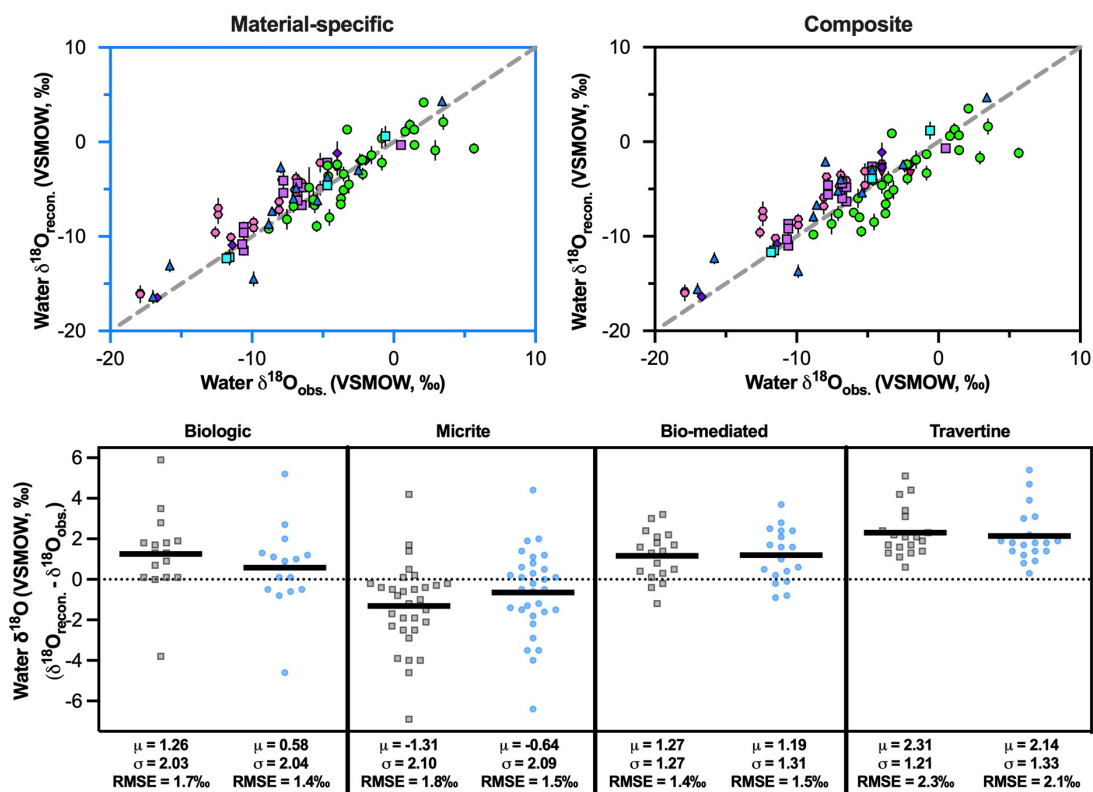
715 **Figure 5: Comparison of reconstructed values of temperature and $\delta^{18}O_{water}$ from material-**
716 **specific and composite calibrations from this study to observations.** Use of a composite Δ_{47}-
717 temperature calibration yields less accurate and precise results. A. Comparison of measured
718 temperature ($T_{obs.}$) to Δ_{47}-derived temperature ($T_{\Delta47}$) values using the material-specific (top row,
719 blue frame) and composite freshwater calibration (top row, black frame). Bottom panel shows a
720 comparison of temperature residuals (reconstructed-observations) using the composite and
721 material-specific calibrations. Values derived using the composite regression are represented
722 using black squares and material-specific calibrations are represented using blue circles.
723 Horizontal black bars represent the mean and values at the bottom of each dataset show the mean
724 value and standard deviation for residuals along with the RMSE for each dataset using the
725 respective calibrations. Our results show improvement in RMSE of reconstructed temperatures
726 for biogenic carbonates and micrites when applying the material specific calibration compared to
727 the composite calibration. Temperature residuals for biologically mediated carbonates are similar
728 between the composite and material specific calibration, however, there is increased spread when
729 applying the material specific calibrations, reflected in the elevated RMSE relative to the
730 composite calibration. Similar to biologically mediated carbonates, the spread in temperature
731 residuals for travertines, and thus RMSE, increases, when using material specific calibrations.
732 However, we note that the overall mean of the residuals is reduced for travertines when applying
733 a material specific calibration relative to the composite calibration. B. Comparison of measured
734 $\delta^{18}O_{water}$ ($\delta^{18}O_{obs.}$) to Δ_{47}-derived $\delta^{18}O_{water}$ values ($\delta^{18}O_{recon.}$) using material specific (top row,
735 blue frame) and composite freshwater calibration (top row, black frame). $\delta^{18}O_{water}$ values are
736 calculated using temperatures derived using our composite and material-specific calibrations
737 between Δ_{47} and temperature, and oxygen isotope mineral-water fractionation factors from Kim
738 and O'Neil (1997) (calcite) or Kim et al. (2007) (aragonite). Bottom panel displays $\delta^{18}O_{water}$
739 residuals (reconstructed-observations) using the composite and material-specific calibrations.
740 Our results show improvement in RMSE for $\delta^{18}O_{water}$ reconstructions for biogenic carbonates,
741 micrites, and travertines. $\delta^{18}O_{water}$ RMSE for biologically-mediated carbonates is similar for both
742 the composite and material specific calibration, however, we note that the mean of the residuals
743 is reduced, and closer to zero, in the material specific calibration.

744   3.3 Reconstructing water $\delta^{18}O$

745   In addition to providing thermodynamic constraints on the temperature of formation of
746 carbonates, Δ_{47} measurements can be paired with carbonate oxygen isotope ratios to directly
747 calculate source water $\delta^{18}O$. We compare our clumped-isotope derived estimates of source water
748 $\delta^{18}O$ derived with our temperature predictions ($\delta^{18}O_{w\text{-reconstructed}}$) to measured modern freshwater
749 $\delta^{18}O$ ($\delta^{18}O_{w\text{-measured}}$) values to evaluate if this method can accurately reconstruct the isotopic
750 composition of the water in which the carbonate precipitated. For $\delta^{18}O_{w\text{-measured}}$, we synthesized
751 any available published measurements for the water bodies examined to compare to
752 reconstructed values. $\delta^{18}O_{w\text{-measured}}$ data is available for 86 of the 108 sites examined in this study
753 (Supplementary Table 4). Although some sites had long-term measurements of water body
754 oxygen isotope composition, some of the measurements were single point measurements, and
755 thus may not fully represent temporal variability.

756   We used the equation of Kim & O'Neil (1997) for calcite and Kim et al. (2007) for
757 aragonite in order to constrain the relationship between formation temperature, $\delta^{18}O_{carbonate}$, and
758 $\delta^{18}O_{water}$. We observe a positive relationship between measured and clumped-isotope derived
759 $\delta^{18}O_{w\text{-reconstructed}}$ derived from the composite freshwater calibration in this study (p = <0.0001; r^2 =
760 0.7935) and material-specific reconstructed temperatures (p <0.0001; r^2 = 0.8267). Figure 4c
761 shows comparison of the residuals for reconstructed $\delta^{18}O_w$ using both the material specific and
762 composite calibrations developed within this study. RMSE was reduced using the material
763 specific calibration relative to the composite calibration for biogenic carbonates (material
764 specific RMSE = 1.5‰, composite RMSE = 1.8‰), micrites (material specific RMSE = 1.4‰,
765 composite RMSE = 1.7‰), and travertines (material specific RMSE = 2.1‰, composite RMSE
766 = 2.3‰). However, for biologically mediated carbonates, the composite calibration slightly
767 outperforms the material specific calibration (material specific RMSE = 1.4‰, composite RMSE
768 = 1.5‰), although the mean of the residuals is closer to zero.

769   Overall, material-specific calibrations perform better at reconstructing $\delta^{18}O_{w\text{-measured}}$
770 (Figure 5). Out of the 87 samples from sites with measured $\delta^{18}O_{water}$ values, 33 samples fall
771 within ±1‰ of hydrographic data when using the material-specific calibrations, a 7%
772 improvement from using the composite calibration (Fig. 5). $\delta^{18}O_{w\text{-reconstructed}}$ values for biologic
773 samples generally recover $\delta^{18}O_{w\text{-measured}}$ within 2‰. However, this method yields, for micrites,
774 lower $\delta^{18}O_{water}$ values than observations for more enriched $\delta^{18}O_{w\text{-measured}}$ values, which could be
775 due to either kinetic effects and/or changes in surface water chemistry during carbonate
776 precipitation events (Fig. 5). If the latter, it is unlikely to be due to evaporative enrichment of
777 $\delta^{18}O_{water}$ which would produce the opposite trend, but it may arise from changes in carbonate
778 chemistry. Biologically-mediated carbonates and travertines show a positive offset from the 1:1
779 line, overestimating $\delta^{18}O_{water}$ relative to the measured value, that may also arise from pH related
780 effects on isotopic fractionation or kinetic isotope effects (e.g., Beck et al., 2005; Tripati et al.,
781 2015).

782   3.4 Comparison of multiple materials at individual sites

783   Five sites in this study contain a combination of two different types of materials
784 analyzed. Three sites in China (Daija Co, Cuona Lake, and Wulungu Lake) have micrite (Li et
785 al., 2021) and freshwater mollusks (this study), and both the North Arm and the South Arm of
786 the Great Salt Lake in Utah contain modern microbialite and ooid samples (Pace et al., 2016).
787 Comparing results from different carbonate types provides another method of assessing overall

788   calibration performance, therefore we compare clumped isotope-derived water temperature
789   estimates using both material-specific and our composite freshwater calibrations at these sites
790   where different materials are present.

791   Figure 6 shows increased agreement between different sample types for the same location
792   for temperature and water $\delta^{18}O$ in a majority of cases when a material-specific calibration is
793   used. The lakes in China containing dual-materials are terminal lakes where authigenic carbonate
794   precipitation is expected to occur in the later part of summer, when temperatures are most
795   elevated and carbonate supersaturation occurs in the surface waters (Hren & Sheldon, 2012).
796   Both Daija Co and Cuona Lake are high elevation lakes (>4.5 km) where the monthly average air
797   temperature doesn't exceed 0°C until May, thus, temperature requirements for mollusk and
798   micrite growth are met during similar conditions, yielding similar estimated temperatures
799   between both archives when using the material-specific calibrations. However, applying our
800   composite calibration to samples in these lakes results in higher calcification temperatures
801   projected for mollusks relative to the micrite. We find more of a disparity between Δ_{47}-derived
802   and directly measured temperature values when taking into account material type at Wulungu
803   Lake, an inland, low elevation and high latitude (47°N) lake with a large range of intra-annual
804   temperatures (~36°C), however, our estimates of water temperature are in agreement with typical
805   seasonality of precipitation from the two archives given the lake's setting. Our results using a
806   material specific calibration suggest that micrite precipitated during a more narrow interval, with
807   higher temperatures and $\delta^{18}O$ values than the mollusk samples, consistent with temperature-
808   induced carbonate precipitation and evaporative enrichment. The temperatures recorded by
809   mollusks at the same lake using the material specific calibrations suggest that the shells may be
810   reflecting dominant calcification during comparatively cooler temperatures in spring or early
811   summer.

812   Modern microbialite and ooid samples from the Great Salt Lake yield similar results,
813   with a 1.5°C difference between archives in both the North and South Arms using the material
814   specific calibration. Both archives in the Northern and Southern arms of the lake are consistent
815   with summer water temperatures when taking into account material type. Furthermore, the
816   separation of the North and South arms of the Great Salt Lake by a causeway results in a more
817   restricted Northern arm with less freshwater input from rivers and more evaporation (Gwynn,
818   2007). Our Δ_{47}-derived temperature data also shows that our carbonate samples from the Great
819   Salt Lake record more elevated heating in the North Arm relative to the South Arm when using
820   the material specific (0.6°C) compared to the composite (0.1°C) calibrations. Further study is
821   needed to fully understand the differences in calcification in between archives in the same
822   settings, but these findings may support the use of a material-specific calibration when
823   developing reconstructions from multiple types of carbonates for ancient freshwater systems.

a. Water temperature

b. Water δ^{18}O

824
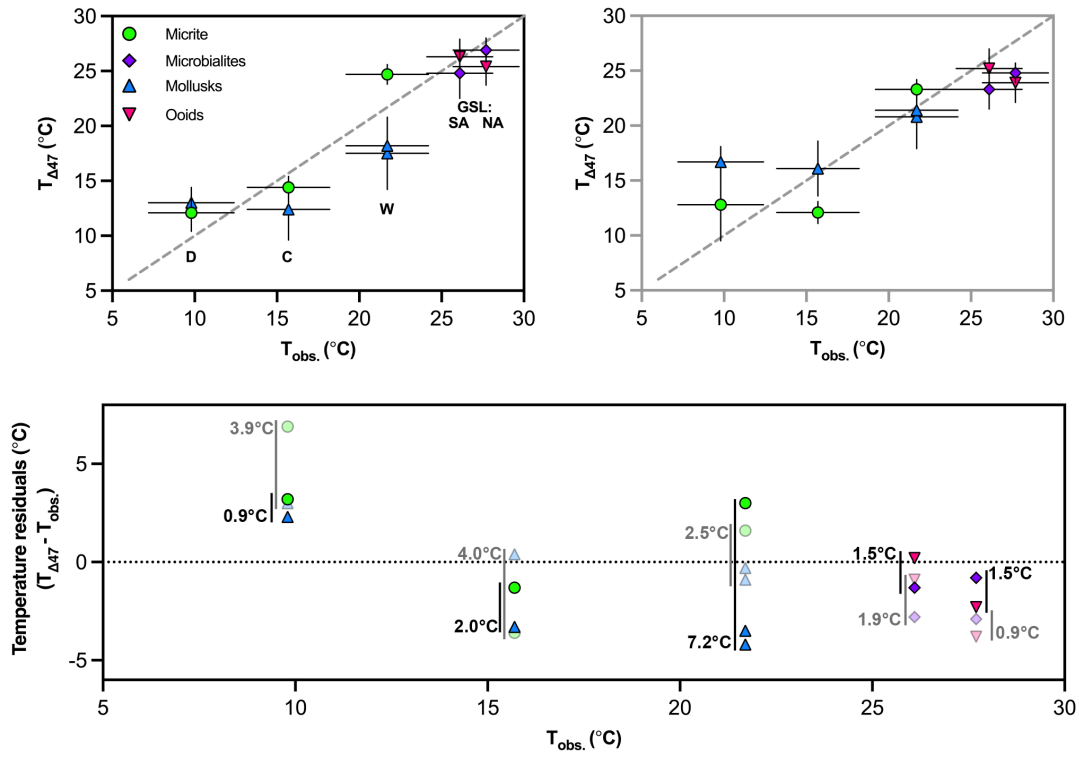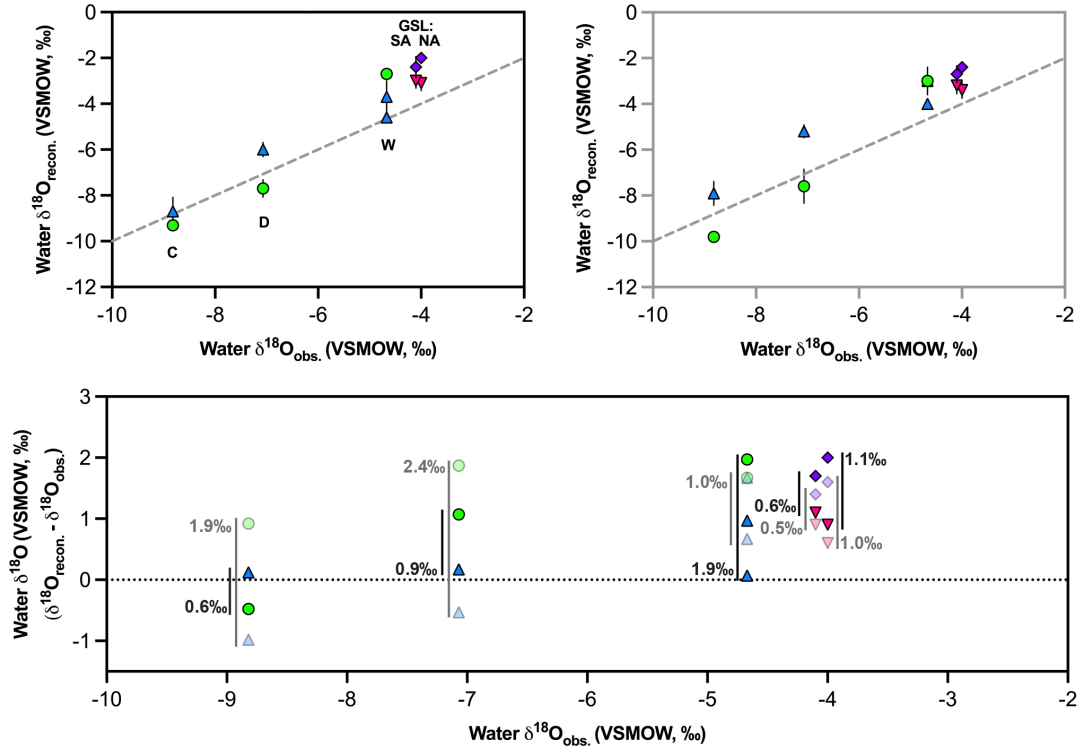
825 **Figure 6: Evaluation of clumped isotope derived temperature and $\delta^{18}O_{water}$ for locations**
826 **with dual materials.** A. Clumped-isotope derived temperature reconstructions using material
827 specific calibrations (top row; black frame) and composite freshwater calibration (top row; gray
828 frame). Bottom panel shows residuals for both the material specific calibrations and composite
829 calibrations (semi-transparent symbols), along with the average difference in temperature
830 between the two archives (black and gray numbers and lines for material specific and composite
831 calibration, respectively). Clumped isotope derived temperatures are denoted as $T_{\Delta47}$, while
832 independently observed water temperatures are denoted as $T_{observations}$. Sites are labeled on plot:
833 D: Daija Co, C: Cuona Lake, W: Wulungu Lake, GSL NA: North Arm, Great Salt Lake, GSL
834 SA: South Arm, Great Salt Lake. We find a reduction of temperature residuals in most cases
835 using a material specific calibration. We also find more realistic temperature estimates when
836 applying material specific calibrations, given each lake's individual setting. B. Reconstructed
837 water $\delta^{18}O$ values using material specific (top row, black frame) and composite (top row, gray
838 frame) calibrations. Clumped isotope based reconstructions of water $\delta^{18}O$ and independently
839 measured $\delta^{18}O$ values are denoted as water $\delta^{18}O_{reconstructed}$ and water $\delta^{18}O_{observed}$, respectively. The
840 residuals from measured values are displayed on the bottom plot, and residuals between different
841 archives are denoted by black and gray bars and values for the material specific and composite
842 calibrations, respectively.

843   3.5 Applications to Paleoclimate Reconstructions

844   3.5.1 Paleoclimatology of Lake Surprise, CA

845   We applied the calibration relationships derived within this study to reconstruct terrestrial
846   paleo-hydroclimate variables, using samples of tufa that are Last Glacial Maximum (LGM;
847   23,000-19,000 years ago) and deglacial (19,000-11,000 years ago) in age from Lake Surprise,
848   California (Egger et al., 2018; Ibarra et al., 2014; Santi et al., 2019; Santi et al., 2020). In the
849   original study from Ibarra et al. (2014), the authors used pollen data to estimate temperature
850   changes during the LGM and deglacial. These estimates were used within an isotope mass
851   balance model to derive evaporation and precipitation rates at Lake Surprise. Santi et al. (2020)
852   expanded on this work by providing further constraints on water temperatures (and air
853   temperatures, by use of a transfer function) and $\delta^{18}O_{water}$ for the same sample set and used these
854   updated values within an isotope mass balance modeling framework to derive new estimates of
855   evaporation and precipitation rates. Here, we applied our biologically-mediated and composite
856   calibrations and the recently published calibration by Anderson et al. (2021) to data from tufa
857   samples for Lake Surprise from Santi et al. (2020). Data used from Lake Surprise is identical to
858   the original publication and was reprojected into the I-CDES reference frame following current
859   best practices and standardization procedures (Bernasconi et al., 2021; Upadhyay et al., 2021).
860   Detailed methodology can be found in Santi et al. (2020) and equations used for this analysis can
861   be found in the Supplementary Information.

862   New estimates of Δ_{47}-temperatures, water $\delta^{18}O$, evaporation, and precipitation rates are
863   shown in Supplementary Figure 1, and reported in Supplementary Table 5, 6, and 7 using the
864   material-specific and composite calibrations derived in this study, and the Anderson et al. (2021)
865   calibration, respectively. Updated temperature predictions using our biologically-mediated
866   calibrations generally result in cooler water temperatures throughout the LGM and deglacial at
867   Lake Surprise than the original publication (Table 4). Water temperatures derived using the
868   Anderson et al. (2021) calibration are 1.2 and 1.7°C cooler than the material-specific calibration,
869   during the deglacial and LGM, respectively. Estimates derived using the general calibration are
870   warmer than the material specific calibration, but slightly cooler than the original publication,
871   with water temperatures estimated to be 12.5 ± 1.1°C during the LGM and 11.4 ± 0.7°C during
872   the deglacial. Average LGM water temperatures of 11.5 ± 1.4°C are estimated using the
873   biologically-mediated calibration, which results in temperatures that are 1.2°C cooler than the
874   originally reported value (Santi et al., 2020) of 12.8 ± 1.4°C. Using the same water-to-air
875   temperature transfer function (Hren & Sheldon, 2012) as used in Santi et al. (2020) to translate
876   water temperatures to LGM MAAT, we find a 3.0°C difference between the material-specific
877   values and published values (1.8 ± 1.9°C and 4.8 ± 1.3°C, respectively). The composite
878   calibration estimates similar temperatures to the original publication (3.2 ± 1.5°C), while the
879   Anderson et al. (2021) calibration estimates much cooler temperatures during the LGM (-0.5 ±
880   1.7°C). Our deglacial MAAT estimates follow a similar trend, with estimates from Santi et al.
881   (2020) resulting in the highest MAAT estimates, followed by our composite calibration, the
882   biologically-mediated calibration, and the Anderson et al. (2021) calibration (Table 4).

883   MAAT estimates were used to calculate annual evaporation rate, using a modified
884   Penman equation (Linacre, 1993; Mering, 2015; Santi et al., 2020). Therefore, shifts in
885   temperature will dictate the direction and magnitude of changes in estimated lake evaporation
886   rate. When using temperatures derived from our material-specific calibrations, we observe a 91

887 mm difference in evaporation in our reanalyzed data (981 ± 60 mm/yr) and the original
888 publication (1072 ± 56 mm/yr) during the deglacial. Our estimates during the LGM are 50
889 mm/yr lower than estimates from Santi et al. (2020), with our results suggesting 1103 ± 115
890 mm/yr and 1153 ± 100 mm/yr, respectively. Our derived weighted evaporation rate, which takes
891 into account free evaporation over the lake surface and evapotranspiration over land, differs
892 significantly from Santi et al. (2020), with a 46 mm/yr decrease and 41 mm/yr increase
893 difference between the new and old estimates for the LGM and deglacial, respectively (Table 4).
894 Since we observe general decreases in temperature using the Anderson calibration, overall,
895 weighted and unweighted evaporation values are lower than those derived in the original
896 publication, while the agreement in temperature from the composite calibration derived
897 evaporation estimates are similar to the original publication (Supplementary Tables 6 and 7).

898 Evaporation estimates are used within the hydrological modeling framework of Santi et
899 al. (2020) to reconstruct precipitation that incorporates clumped isotope derived MAAT and
900 $\delta^{18}O_{water}$ and includes basin hypsometry derived from modern topography and watershed
901 delineations (Broecker, 2010; Ibarra et al., 2014, 2018; Jones et al., 2007; McGee et al., 2018).
902 We also incorporate an ice-volume correction for $\delta^{18}O_{water}$ during the LGM and deglacial based
903 on sample age, following the approach used by Tripati et al. (2014) and estimate anomalies with
904 a revised value for modern annual precipitation rates to account for snowfall. In Santi et al.
905 (2020), modern annual precipitation values used to calculate anomalies used a snow water
906 equivalent of 1:10 mm. However, snow densities vary depending on temperature and location.
907 To account for these changes in snow density, we utilized 10 years of SNOTEL snow density
908 data (USDA Natural Resources Conservation Service, 2022) at two stations within the Surprise
909 basin (Cedar's Pass and Dismal Creek) to assess typical modern snow water equivalent in
910 Surprise Valley. The average snow density for the area was 33%, and we combined this value
911 with average snowfall amounts to integrate the contribution derived from snow into our modern
912 precipitation measurements, for an updated modern precipitation value of 630 mm/year (Desert
913 Research Institute; https://www.dri.edu/western-regional-climate-center/), a 102 mm/year
914 increase.

915 These updated calculations using the material-specific calibration indicate that during the
916 LGM, precipitation rates were 10% lower than modern, and precipitation increased during the
917 deglacial to values that were 8% lower than today (Table 4). Estimates of precipitation rates
918 using all calibrations are similar, with estimates for the LGM ranging from 551 to 565 mm/yr
919 (Table 4). We observe a slight increase in precipitation rate estimates when applying all
920 calibrations during the deglacial, when Lake Surprise reached its maximum extent, with values
921 using the original published calibration resulting in estimates of 567 mm/yr, which is 16, 1, and 8
922 mm/year lower than estimates derived from our material-specific, composite, and the Anderson-
923 derived values, respectively. Overall, this supports the original findings of Ibarra et al. (2014)
924 and those of Santi et al. (2020) based on clumped isotopes that temperature and evaporation were
925 likely dominant controls on Lake Surprise's transgression and regression, and that increased
926 evaporation relative to precipitation contributed to the eventual disappearance of Lake Surprise.

Hydroclimate reconstruction at Lake Surprise, CA

(41.5°N, 120.0°W)	MAAT (°C)		$\delta^{18}O_w$ (‰)		Precipitation (mm/yr)		Weighted Evaporation (mm/yr)	
	LGM	**Deglacial**	**LGM**	**Deglacial**	**LGM**	**Deglacial**	**LGM**	**Deglacial**
This study - material-specific	1.8 ± 1.9	0.1 ± 1.3	-2.9 ± 0.3	-3.3 ± 0.2	565 ± 50	582 ± 14	635 ± 46	627 ± 28
This study - composite	3.2 ± 1.5	1.8 ± 1.0	-2.7 ± 0.3	-3.0 ± 0.2	551 ± 23	566 ± 15	633 ± 46	631 ± 27
Anderson et al. (2021)	-0.5 ± 1.7	-1.6 ± 1.1	-3.3 ± 0.3	-3.6 ± 0.2	558 ± 18	573 ± 12	597 ± 37	593 ± 18
Santi et al. (2020)	4.8 ± 1.3	3.8 ± 0.9	-2.7 ± 0.3	-2.4 ± 0.2	552 ± 24	566 ± 16	647 ± 44	655 ± 27

	Temperature Anomaly (°C)		$\delta^{18}O_w$ Anomaly (‰)		Precipitation Anomaly (%)		Weighted Evaporation Anomaly (%)	
	LGM	**Deglacial**	**LGM**	**Deglacial**	**LGM**	**Deglacial**	**LGM**	**Deglacial**
This study - material-specific	-7.4 ± 2.1	-9.1 ± 1.6	11.6 ± 0.7	11.2 ± 0.6	-10 ± 26	-8 ± 26	20 ± 9	19 ± 6
This study - composite	-6.0 ± 1.8	-7.4 ± 1.4	11.8 ± 0.7	11.5 ± 0.6	-12 ± 26	-10 ± 26	20 ± 9	19 ± 5
Anderson et al. (2021)	-9.7 ± 2.0	-10.8 ± 1.5	11.2 ± 0.7	10.9 ± 0.6	-11 ± 26	-9 ± 26	28 ± 6	33 ± 6
Santi et al. (2020)	-4.4 ± 1.6	-5.4 ± 1.3	12.1 ± 0.6	11.8 ± 0.7	-12 ± 26	-10 ± 26	22 ± 9	24 ± 6

Elevation reconstruction in Nangqian Basin, Tibetan Plateau

(32.2°N, 96.5°E)	Unit 1 (mid Cretaceous)		Unit 3 (mid Paleogene; >38 Ma)		Unit 4 (38-37 Ma)		
	T_w (°C)	$d^{18}O_w$ (‰)	T_w (°C)	$\delta^{18}O_w$ (‰)	T_w (°C)	$\delta^{18}O_w$ (‰)	Elevation (km)
This study - material-specific	25.1 ± 3.0	-6.0 ± 1.2	39.0 ± 3.7	-5.0 ± 0.8	29.0 ± 3.5	-6.2 ± 1.1	2.9 ± 1.1
This study - composite	23.7 ± 3.3	-6.3 ± 1.0	38.8 ± 4.1	-5.0 ± 0.7	27.9 ± 3.8	-6.5 ± 1.0	2.9 ± 1.1
Anderson et al. (2021)	21.7 ± 3.4	-6.7 ± 1.0	37.7 ± 4.4	-5.2 ± 0.8	26.1 ± 4.0	-6.8 ± 1.0	3.0 ± 1.1
Li et al. (2019)	24.9 ± 2.8	-6.2 ± 1.5	40.9 ± 4.1	-4.6 ± 0.9	29.7 ± 3.7	-6.2 ± 1.4	3.0 ± 1.1

927

928 **Table 4: Comparison of recalculated Δ_{47}-based proxy reconstructions from this study to**
929 **published values.** Top: Comparison of water temperature, water $\delta^{18}O$, precipitation, and
930 weighted evaporation anomalies at Lake Surprise, CA to published values from Santi et al.
931 (2020). Modern MAAT is $9.2 \pm 1.0°C$ from Cedarville, CA and modern $\delta^{18}O$ used for anomaly
932 calculations is $-14.6 \pm 0.6‰$. Modern precipitation used to calculate the anomaly is 630
933 mm/year, including contributions from rainfall and snowmelt, and modern evapotranspiration
934 rates are 528 mm/year. Bottom: Comparison of clumped isotope derived water temperature,
935 water $\delta^{18}O$, and elevation estimates for samples run for clumped isotope analysis from the
936 Nangquian Basin to published values from L. Li et al. (2019).

937   3.6.2. Origin of travertine and tufa deposits in Ainet, Austria

938   We apply our calibrations to study the formation of travertines and tufas in a
939 mountainous region of the Alps. To demonstrate this, we examined a lateglacial sequence of
940 travertine and calcareous tufa from Ainet, Austria that was first described in Boch et al. (2005).
941 It represents the only aragonitic travertine sequence known in the Eastern Alps. This sequence of
942 ~2.7 m thickness formed over the course of ~1,000 years, following the rapid initiation of
943 warming during the Bølling-Allerød (Figure 7). Carbonate deposition within the travertine
944 sequence alternated between aragonite and calcite layers (on mm-scale), which was hypothesized
945 to represent differences in seasonality, with aragonite precipitation occurring during the warm
946 season and calcite precipitation occurring during cooler intervals. Following the deposition of the
947 compact and aragonite dominated travertine (~2.5 m), this sequence was then capped by a highly
948 porous and calcareous tufa layer (~0.2 m) consisting of calcite solely.

949   Here, we constrain formation temperature and $\delta^{18}O_{water}$ for these differentiated calcium
950 carbonates using our biologically-mediated and travertine calibrations from this study.
951 Temperature estimates for the tufa and travertine sequence range from 9.0 to 15.1°C, with an
952 average value of 12.7°C for the travertine terrace (Supplementary Table 8). Modern water
953 temperatures taken in May, July, and October range from 6.6 - 12.2°C, similar to our Δ_{47}-derived
954 estimates. Although the initial study suggested a seasonal control on aragonite and calcite
955 formation, with aragonite being precipitated in the warmer months and calcite being precipitated
956 in the cooler months, we do not resolve a clear relationship between temperature and mineralogy
957 within this limited dataset (Figure 7).

958   Our Δ_{47}-temperatures and $\delta^{18}O_{water}$ values support the hypothesis that the travertine
959 sequence did not have a hydrothermal origin (thermal water discharge), but are consistent with
960 being derived from rapid CO_2 degassing from groundwater discharge of meteoric origin, with
961 sufficient time for dissolved inorganic carbon equilibration to occur. We observe consistency
962 between modern $\delta^{18}O_{water}$ values measured from a series of nearby streams (-11.5 to -12.1‰
963 VSMOW) and $\delta^{18}O_{water}$ estimates derived from clumped isotope analysis (-11.4 to -12.2‰
964 VSMOW). Given this consistency in $\delta^{18}O_{water}$, we suggest recharged meteoric groundwater
965 (seasonal rainfall, snowmelt) and eventually some contribution from ice melting due to a rapid
966 increase in temperatures during the Bølling-Allerød is likely to have been the surface dominated
967 paleofluid source for carbonate precipitation here. The calcium carbonate source of the
968 freshwater carbonate precipitates is probably manifested in local marble lenses within the
969 prevalent metamorphic rocks and additional CO_2 from underground might have been dissolved
970 in the percolating groundwaters favored by deep-seated slope displacements (as a consequence
971 of glacial ice melting) and faults that have been locally detected (Boch et al., 2005).

972   The analysis of this travertine sequence illustrates the importance of an appropriate
973 calibration selection. While application of our composite freshwater carbonate calibration would
974 yield temperature values 2.5 - 2.7°C higher than modern streamflow, use of the material-specific
975 travertine calibration yields formation temperatures more similar to modern stream temperatures
976 (Supplementary Table 8), which are more likely to be correct for carbonates forming in an
977 interval of distinct relative warmth in the last glacial period. The $\delta^{18}O_{water}$ values reconstructed
978 from the material-specific calibration are within error of modern groundwater values, measured
979 from spring-fed streams, while reconstructed $\delta^{18}O_{water}$ values are 0.5 to 0.6‰ higher when using
980 the composite calibration relative to the material-specific calibration. We note the Anderson et

981   al. (2021) calibration estimates the formation temperature of the calcareous tufa sample to be

982   9.1°C, 1.6°C colder than the temperatures calculated using the biologically mediated calibration.

983   The cooler temperature estimated by Anderson et al. (2021) results in $\delta^{18}O_{water}$ that are 0.4‰

984   more depleted relative to the biologically mediated calibration. Reconstructed temperatures and

985     $\delta^{18}O_{water}$ values for the travertine sequence using the Anderson et al. (2021) calibration result in

986   temperature values that are similar to our travertine calibration (0 - 0.2°C higher) and identical

987     $\delta^{18}O_{water}$ values. Given that the travertine calibration is indistinguishable from the Anderson et al.

988   (2021) calibration according to an ANCOVA test (slope: $p = 0.6320$; intercept: $p = 0.4440$), the

989   similarities in temperatures and $\delta^{18}O_{water}$ values between the two calibrations is unsurprising.

990
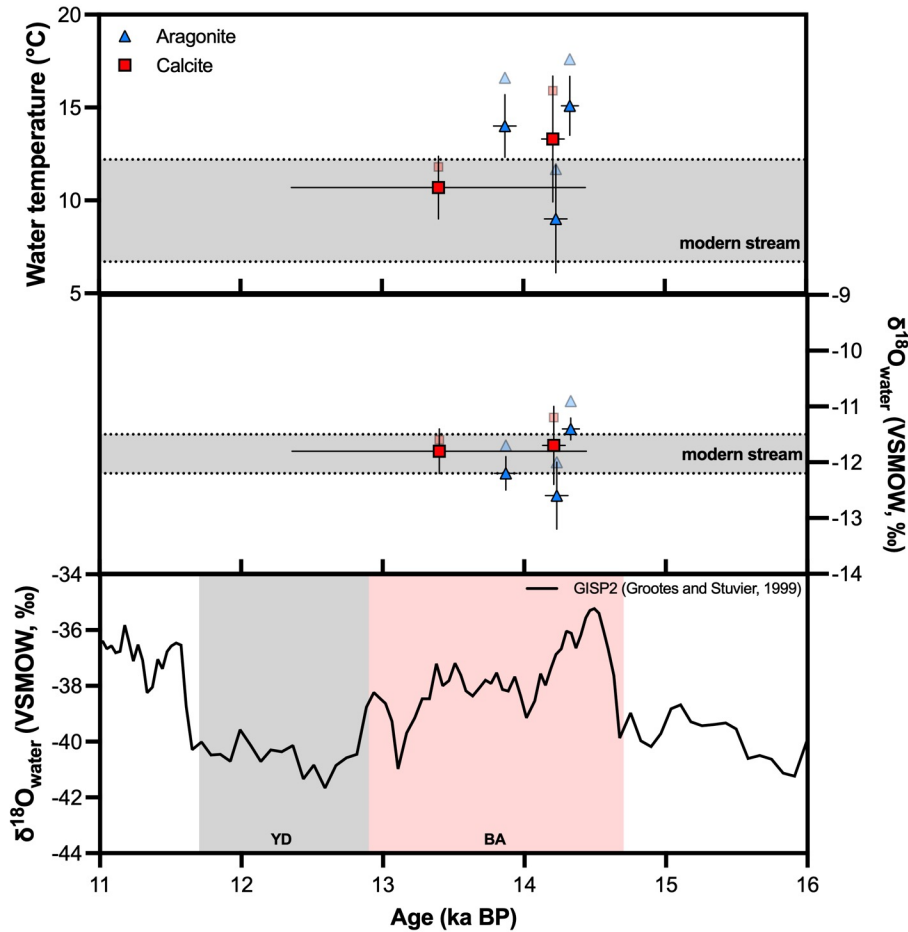
Figure 7: Clumped isotope derived estimates of temperature and δ¹⁸O_water for a travertine terrace in Ainet, Austria. Solid symbols represent estimates derived from material-specific calibrations, while lighter symbols represent estimates derived from our composite freshwater calibration. Gray bands represent the range of modern stream values measured in May, July, and October (Boch et al., 2005) and data for GISP2 ice core record is from Stuiver and Grootes (2000). Values are broadly consistent with modern temperatures and δ¹⁸O_water of nearby streams. Seasonally enhanced percolation of meteoric waters and melting of the last glacial Alpine glaciers during initiation of the pronounced Bølling-Allerød warm period are hypothesized to have recharged groundwater via new flow routes (slope failure/graben and faults) opening during the melting phase and promoting the relatively short lived discharge and calcium carbonate precipitation event.

1002   3.6.3 Application to Paleoaltimetry

1003   Following on stable isotope and leaf margin-based paleoaltimetry (Blisniuk & Stern,
1004   2005; Gregory-Wodzicki, 2000; McElwain, 2004; Rowley & Garzione, 2007; Wolfe et al.,
1005   1998), clumped isotope analyses have been used to constrain the tectonic history of a region
1006   (Ghosh, Garzione, et al., 2006; Huntington & Lechler, 2015; L. Li et al., 2019; Quade et al.,
1007   2013). This proxy relies on the premise that lake water temperature is directly related to air
1008   temperature; therefore, as basins undergo surface uplift as a result of large-scale tectonic
1009   processes (e.g., crustal shortening and thickening, convective removal of lower lithosphere, etc.),
1010   the ambient air and water temperature should decrease, as governed by the local lapse rate
1011   (Ghosh, Garzione, et al., 2006; Huntington & Lechler, 2015; L. Li et al., 2019; Quade et al.,
1012   2013). Reconstructed $\delta^{18}O_{water}$ can provide additional constraints on paleoelevation, because the
1013   stable isotope compositions of meteoric and surface waters decreases as altitude increases
1014   (Chamberlain & Poage, 2000; Poage & Chamberlain, 2001; Rowley & Garzione, 2007). To
1015   assess the impact of our calibrations on a published paleoelevation reconstruction for the Tibetan
1016   Plateau, we recalculate temperatures and $\delta^{18}O_{water}$ estimates from L. Li et al. (2019) using the
1017   micrite, composite, and Anderson et al. (2021) calibration for lacustrine samples in the Nangqian
1018   Basin. We used our clumped-isotope derived results to compare estimates of elevation changes
1019   during the late Eocene following the methodology used in the original publication.

1020   Overall, the micrite calibration equation derives similar temperatures for unaltered
1021   carbonates to those derived in the original publication using the Kelson calibration
1022   (Supplementary Table 9). Mean temperatures for Units 1, 3, and 4 using the new calibration
1023   derived in this study are 25.1 ± 3.0, 39.0 ± 3.7, and $29.0 \pm 3.5°C$. These values are 0.2°C higher,
1024   1.9°C lower, and 0.7°C lower than published results, respectively. The general calibration
1025   estimates slightly cooler values than our material-specific derived results (1.4, 0.2, and 1.1°C
1026   lower for Units 1, 3, and 4, respectively). The Anderson calibration projects even cooler values,
1027   with Units 1, 3, and 4 estimates being 3.4, 1.2, and 3.4°C lower, respectively.

1028   In the new calibration, samples from Unit 2 yield high temperatures between 44.2 and
1029   67.8°C, which agree with previous observation and interpretation of deep burial diagenetic
1030   alteration of the Unit 2 samples (L. Li et al., 2019). We also note that the previous interpretation
1031   for the new temperatures of Unit 1 still holds, such that the lower temperatures in the Late
1032   Cretaceous represent either less heating of lake water or possibly higher surface elevation in the
1033   Nangqian Basin.

1034   Late Eocene (38-37 Ma) carbonates analyzed from Unit 4 were suggested to be deposited
1035   near-surface and their Δ_{47}-temperature values were used to reconstruct $\delta^{18}O_{water}$ values and
1036   paleoelevation (L. Li et al., 2019). We calculate similar values using our calibration for late
1037   Eocene highland water $\delta^{18}O$ values to be -9.4‰ and -9.8‰, respectively, compared to -9.1‰ and
1038   -9.8‰ in the original study. Following the method in L. Li et al. (2019) where the authors use
1039   different modeling approaches to consider dominant regional moisture sources, the paleo-water
1040 $\delta^{18}O$ values correspond to a mean hypsometric paleoelevation of 2.8 ± 1.1 km and 3.1 ± 1.1 km,
1041   which is very similar to the reconstruction that was published (2.8 ± 1.1 km and 3.2 ± 1.1 km), and
1042   ~1.3 km lower than the modern hypsometric mean elevation (4.2 km) of the Nangqian Basin.
1043   Given the similarities in projected water temperatures between the material-specific and
1044   composite regressions for the sample used to reconstruct paleoelevation, it is unsurprising that
1045   the projected elevation estimates are identical (Table 4). The cooler temperatures derived using
1046   Anderson calibrations result in more depleted water $\delta^{18}O$ values (-9.5‰ and -10.0‰) and

1047 slightly higher estimates of paleoelevation (2.9±1.1 km and 3.2±1.1 km), but still within error of
1048 the original publication and findings in this study.

1049   The basin floor paleoelevation of the Nangqian Basin was estimated from the T-Δ_{47}
1050 values of late Eocene lacustrine carbonate in unit 4. The newly calculated mean T-Δ_{47} value of
1051 these samples is 29.5°C, 0.5°C higher than what was published. Following the method in Li et al.
1052 (2019), this mean T-Δ_{47} value is 12.5°C higher than the estimated warm-season lake surface
1053 water temperature (~17°C) for an elevation at 3.8 km. Benthic foraminiferal records indicate that
1054 roughly 6°C of the temperature decrease can be attributed to the post-Eocene global cooling
1055 (Hansen et al., 2008), while the remaining 6.5°C reflects paleoelevation increase of the basin
1056 floor after the Eocene. Following the method in L. Li et al. (2019), this indicates 1.1 ± 0.3 km of
1057 post–late Eocene elevation increase, if a lapse rate of -6.1 ± 1.0 °C/km is applied for lake
1058 surface-water temperature on the Tibetan Plateau (Huntington et al., 2015). Therefore, the late
1059 Eocene elevation of the Nangqian Basin floor is estimated as 2.7 km above sea level, which is
1060 1.1 km lower than the modern elevation of 3.8 km.

1061 **4 Conclusions**

1062   In order to confidently use proxies to characterize and understand past environments, it is
1063 necessary to have a solid understanding of modern systems. Thus, in this work, we present an
1064 extensive composite dataset of 135 clumped isotope samples of terrestrial freshwater carbonates
1065 from 96 sites, and derive relationships between modern water temperatures and Δ_{47}. These
1066 freshwater Δ_{47}-temperature calibrations are well constrained, encompass a variety of types of
1067 natural lacustrine, fluvial, and spring carbonates, and span a broad range of temperatures,
1068 elevations, and latitudes. As the carbonates presented in this study are taken directly from
1069 modern freshwater settings, they are more representative of real-world systems, and may, in
1070 some circumstances, be more appropriate for application to reconstruct paleotemperatures, than
1071 synthetically-derived Δ_{47}-temperature carbonate calibrations. However, we note that since our
1072 approach utilizes *in-situ* lake water surface temperature data, there is an added uncertainty in the
1073 timing of carbonate formation temperature and calcification timeframe for each of our calibration
1074 samples.

1075   Our results show a convergence of slopes but differences in the intercepts of the Δ_{47}-
1076 temperature relationship between freshwater carbonate groups. Specifically an ANCOVA
1077 analysis shows that material specific calibrations based on grouping freshwater carbonates
1078 (biogenic, biologically mediated, micrite, and travertine) have statistically indistinguishable
1079 slopes between other freshwater carbonate groups and recently published calibration studies, but
1080 in some cases, where there is strong evidence for biogenicity, detects differences in intercepts.

1081   Utilizing a single, composite calibration does not always yield the most accurate results,
1082 while in most cases, implementing material-specific calibrations reduces the magnitude of
1083 residuals (offsets between Δ_{47}-derived temperatures/water $\delta^{18}O$ and measured temperature/water
1084 $\delta^{18}O$) and RMSE, and thus, can provide more robust estimates of temperature. Water $\delta^{18}O$ values
1085 derived from utilizing material specific calibrations can recover independently measured water
1086 $\delta^{18}O$ values accurately, with 39% and 74% of lakes being within 1‰ and 2‰ of measured water
1087 $\delta^{18}O$, respectively, reflecting a 7% and 10% improvement relative to our composite freshwater
1088 calibration.

1089   Additionally, we explore the application of the new calibration relationships reported in
1090   this study by examining three case studies using Δ_{47} measurements of freshwater carbonates.
1091   First, we utilize the biologically-mediated and composite calibrations to explore hydroclimatic
1092   changes from the LGM and deglacial at Lake Surprise in the Western US and derive cooler
1093   temperatures using material-specific, composite, and Anderson calibrations, but with similar
1094   results for evaporation and precipitation rates. Second, we utilize the micrite calibration to
1095   estimate the Eocene paleoelevation of the Nangqian Basin within the Tibetan Plateau and find
1096   that our material-specific derived elevations are in agreement with the original publication, but
1097   elevations derived from the composite and Anderson calibration suggest a higher degree of
1098   uplift. We also present a new dataset from a travertine sequence in Austria and show that the
1099   origin of the fluid that allowed for carbonate formation was likely derived from groundwater
1100   sources due to increased percolation of meteoric water and glacial melt. Overall, this work
1101   provides a basis for more accurate reconstructions of terrestrial paleoclimate, paleohydrology,
1102   and paleoaltimetry using freshwater archives, and opens the door to more robust understandings
1103   of paleoenvironmental processes.

1104   **Acknowledgments**

1118
1119   **Open Research**

1120   Data will be available in the Earth-Chem database, pending acceptance of manuscript.
1121   Sample and replicate level data for restandardized samples will also be archived in the Earth-
1122   Chem database as well as the NCDC Paleoclimatology Database.

1123
1124   **References**

1125   Airo, A. (2010). *Biotic and abiotic controls on the morphological and textural development of*

1126   *modern microbialites at Lago Sarmiento, Chile*. Stanford University, Geological and

1127   Environmental Sciences Department, Ph. D ….

1128   Anadón, P., Cabrera, L., & Kelts, K. (2009). *Lacustrine facies analysis* (Vol. 30). John Wiley &

1129   Sons.

1130   Anderson, N. T., Kelson, J. R., Kele, S., Daëron, M., Bonifacie, M., Horita, J., Mackey, T. J.,

1131   John, C. M., Kluge, T., Petschnig, P., Jost, A. B., Huntington, K. W., Bernasconi, S. M.,

1132   & Bergmann, K. D. (2021). A Unified Clumped Isotope Thermometer Calibration (0.5–

1133   1,100°C) Using Carbonate-Based Standardization. *Geophysical Research Letters*, *48*(7),

1134   e2020GL092069. https://doi.org/10.1029/2020GL092069

1135   Apolinarska, K., Pełechaty, M., & Noskowiak, D. (2015). Differences in stable isotope

1136   compositions of freshwater snails from surface sediments of two Polish shallow lakes.

1137   *Limnologica*, *53*, 95–105. https://doi.org/10.1016/j.limno.2015.06.003

1138   Arenas-Abad, C., Vázquez-Urbez, M., Pardo-Tirapu, G., & Sancho-Marcén, C. (2010). Fluvial

1139   and associated carbonate deposits. *Developments in Sedimentology*, *61*, 133–175.

1140   Beck, W. C., Grossman, E. L., & Morse, J. W. (2005). Experimental studies of oxygen isotope

1141   fractionation in the carbonic acid system at 15, 25, and 40 C. *Geochimica et*

1142   *Cosmochimica Acta*, *69*(14), 3493–3503.

1143   Bernasconi, S. M., Daëron, M., Bergmann, K. D., Bonifacie, M., Meckler, A. N., Affek, H. P.,

1144   Anderson, N., Bajnai, D., Barkan, E., Beverly, E., Blamart, D., Burgener, L., Calmels, D.,

1145   Chaduteau, C., Clog, M., Davidheiser-Kroll, B., Davies, A., Dux, F., Eiler, J., … Ziegler,

1146   M. (2021). InterCarb: A Community Effort to Improve Interlaboratory Standardization of

1147   the Carbonate Clumped Isotope Thermometer Using Carbonate Standards. *Geochemistry,*

1148   *Geophysics, Geosystems*, *22*(5), e2020GC009588.

1149   https://doi.org/10.1029/2020GC009588

1150   Bernasconi, S. M., Müller, I. A., Bergmann, K. D., Breitenbach, S. F. M., Fernandez, A., Hodell,

1151   D. A., Jaggi, M., Meckler, A. N., Millan, I., & Ziegler, M. (2018). Reducing

1152   Uncertainties in Carbonate Clumped Isotope Analysis Through Consistent Carbonate-

1153   Based Standardization. *Geochemistry, Geophysics, Geosystems*, *19*(9), 2895–2914.

1154   https://doi.org/10.1029/2017GC007385

1155   Blisniuk, P. M., & Stern, L. A. (2005). Stable isotope paleoaltimetry: A critical review.

1156   *American Journal of Science*, *305*(10), 1033–1074.

1157   https://doi.org/10.2475/ajs.305.10.1033

1158   Boch, R., Spötl, C., Reitner, J. M., & Kramers, J. (2005). A lateglacial travertine deposit in

1159   Eastern Tyrol (Austria). *Austrian Journal of Earth Sciences*, *98*, 78–91.

1160   Boch, R., Wang, X., Kluge, T., Leis, A., Lin, K., Pluch, H., Mittermayr, F., Baldermann, A.,

1161   Boettcher, M. E., & Dietzel, M. (2019). Aragonite–calcite veins of the 'Erzberg'iron ore

1162   deposit (Austria): Environmental implications from young fractures. *Sedimentology*,

1163   *66*(2), 604–635.

1164   Brady, A. L., Laval, B., Lim, D. S. S., & Slater, G. F. (2014). Autotrophic and heterotrophic

1165   associated biosignatures in modern freshwater microbialites over seasonal and spatial

1166   gradients. *Organic Geochemistry*, *67*, 8–18.

1167   https://doi.org/10.1016/j.orggeochem.2013.11.013

1168   Brenner, M., Whitmore, T. J., Curtis, J. H., Hodell, D. A., & Schelske, C. L. (1999). Stable

1169   isotope (δ13C and δ15N) signatures of sedimented organic matter as indicators of historic

1170   lake trophic state. *Journal of Paleolimnology*, *22*(2), 205–221.

1171   Broecker, W. (2010). Long-term water prospects in the western United States. *Journal of*

1172   *Climate*, *23*(24), 6669–6683.

1173 Capezzuoli, E., Gandin, A., & Pedley, M. (2014). Decoding tufa and travertine (fresh water

1174   carbonates) in the sedimentary record: The state of the art. *Sedimentology*, *61*(1), 1–21.

1175   https://doi.org/10.1111/sed.12075

1176 Chamberlain, C. P., & Poage, M. A. (2000). Reconstructing the paleotopography of mountain

1177   belts from the isotopic composition of authigenic minerals. *Geology*, *28*(2), 115–118.

1178   https://doi.org/10.1130/0091-7613(2000)28<115:RTPOMB>2.0.CO;2

1179 Cheng, F., Garzione, C., Li, X., Salzmann, U., Schwarz, F., Haywood, A. M., Tindall, J., Nie, J.,

1180   Li, L., & Wang, L. (2022). Alpine permafrost could account for a quarter of thawed

1181   carbon based on Plio-Pleistocene paleoclimate analogue. *Nature Communications*, *13*(1),

1182   1–12.

1183 Costa, K. C., Hallmark, J., Navarro, J. B., Hedlund, B. P., Moser, D. P., Labahn, S., & Soukup,

1184   D. (2008). Geomicrobiological Changes in Two Ephemeral Desert Playa Lakes in the

1185   Western United States. *Geomicrobiology Journal*, *25*(5), 250–259.

1186   https://doi.org/10.1080/01490450802153033

1187 Crul, R. (1997). Limnology and hydrology of Lakes Tanganyika and Malawi. *Studies and*

1188   *Reports in Hydrology*, *54*.

1189 Csank, A. Z., Tripati, A. K., Patterson, W. P., Eagle, R. A., Rybczynski, N., Ballantyne, A. P., &

1190   Eiler, J. M. (2011). Estimates of Arctic land surface temperatures during the early

1191   Pliocene from two novel proxies. *Earth and Planetary Science Letters*, *304*(3–4), 291–

1192   299.

1193 Daëron, M. (2021). Full propagation of analytical uncertainties in $\Delta47$ measurements.

1194   *Geochemistry, Geophysics, Geosystems*, *22*(5), e2020GC009592.

1195   Daëron, M., Blamart, D., Peral, M., & Affek, H. P. (2016). Absolute isotopic abundance ratios

1196   and the accuracy of Δ47 measurements. *Chemical Geology*, *442*, 83–96.

1197   https://doi.org/10.1016/j.chemgeo.2016.08.014

1198   Daëron, M., Drysdale, R. N., Peral, M., Huyghe, D., Blamart, D., Coplen, T. B., Lartaud, F., &

1199   Zanchetta, G. (2019). Most Earth-surface calcites precipitate out of isotopic equilibrium.

1200   *Nature Communications*, *10*(1), 1–7.

1201   Davies, A. J., & John, C. M. (2019). The clumped (13C18O) isotope composition of echinoid

1202   calcite: Further evidence for "vital effects" in the clumped isotope proxy. *Geochimica et*

1203   *Cosmochimica Acta*, *245*, 172–189. https://doi.org/10.1016/j.gca.2018.07.038

1204   Dettman, D. L., Palacios-Fest, M. R., Nkotagu, H. H., & Cohen, A. S. (2005). Paleolimnological

1205   investigations of anthropogenic environmental change in Lake Tanganyika: VII.

1206   Carbonate isotope geochemistry as a record of riverine runoff. *Journal of*

1207   *Paleolimnology*, *34*(1), 93–105. https://doi.org/10.1007/s10933-005-2400-x

1208   Dickman, M. (1987). Lake sediment microlaminae and annual mortalities of photosynthetic

1209   bacteria in an oligomictic lake. *Freshwater Biology*, *18*(1), 151–164.

1210   https://doi.org/10.1111/j.1365-2427.1987.tb01303.x

1211   Dong, J., Eiler, J., An, Z., Li, X., Liu, W., & Hu, J. (2021). Clumped isotopic compositions of

1212   cultured and natural land-snail shells and their implications. *Palaeogeography,*

1213   *Palaeoclimatology, Palaeoecology*, *577*, 110530.

1214   https://doi.org/10.1016/j.palaeo.2021.110530

1215   Dunca, E., & Mutvei, H. (2001). Comparison of microgrowth pattern in Margaritifera

1216   margaritifera shells from south and north Sweden. *American Malacological Bulletin*,

1217   *16*(1–2), 239–250.

1218 Eagle, R. A., Eiler, J. M., Tripati, A. K., Ries, J. B., Freitas, P. S., Hiebenthal, C., Wanamaker,

1219   A. D., Taviani, M., Elliot, M., Marenssi, S., Nakamura, K., Ramirez, P., & Roy, K.

1220   (2013). The influence of temperature and seawater carbonate saturation state on 13C–

1221   18O bond ordering in bivalve mollusks. *Biogeosciences*, *10*(7), 4591–4606.

1222   https://doi.org/10.5194/bg-10-4591-2013

1223 Eagle, R. A., Risi, C., Mitchell, J. L., Eiler, J. M., Seibt, U., Neelin, J. D., Li, G., & Tripati, A. K.

1224   (2013). High regional climate sensitivity over continental China constrained by glacial-

1225   recent changes in temperature and the hydrological cycle. *Proceedings of the National*

1226   *Academy of Sciences*, *110*(22), 8813–8818. https://doi.org/10.1073/pnas.1213366110

1227 Egger, A. E., Ibarra, D. E., Weldon, R., Langridge, R. M., Marion, B., Hall, J., Starratt, S. W., &

1228   Rosen, M. R. (2018). Influence of pluvial lake cycles on earthquake recurrence in the

1229   northwestern Basin and Range, USA. *Geological Society of America Special Paper*, *536*,

1230   1–28.

1231 Epstein, S., Buchsbaum, R., Lowenstam, H. A., & Urey, H. C. (1953). Revised carbonate-water

1232   isotopic temperature scale. *Geological Society of America Bulletin*, *64*(11), 1315–1326.

1233 Esper, J., George, S. St., Anchukaitis, K., D'Arrigo, R., Ljungqvist, F. C., Luterbacher, J.,

1234   Schneider, L., Stoffel, M., Wilson, R., & Büntgen, U. (2018). Large-scale, millennial-

1235   length temperature reconstructions from tree-rings. *Dendrochronologia*, *50*, 81–90.

1236   https://doi.org/10.1016/j.dendro.2018.06.001

1237 Feakins, S. J., Kirby, M. E., Cheetham, M. I., Ibarra, Y., & Zimmerman, S. R. H. (2014).

1238   Fluctuation in leaf wax D/H ratio from a southern California lake records significant

1239   variability in isotopes in precipitation during the late Holocene. *Organic Geochemistry*,

1240   *66*, 48–59. https://doi.org/10.1016/j.orggeochem.2013.10.015

1241 Fein, J. B. (2017). Advanced biotic ligand models: Using surface complexation modeling to

1242   quantify metal bioavailability to bacteria in geologic systems. *Chemical Geology*, *464*,

1243   127–136. https://doi.org/10.1016/j.chemgeo.2016.10.001

1244 Ferrero, M., Farías, M. E., & Siñeriz, F. (2004). Preliminary characterization of microbial

1245   communities in high altitude wetlands of northwestern Argentina by determining terminal

1246   restriction fragment length polymorphisms. *Revista Latinoamericana de Microbiologia*,

1247   *46*(3–4), 72–80.

1248 Flügel, E. (2004). *Microfacies of carbonate rocks: Analysis, interpretation and application*.

1249   Springer Science & Business Media.

1250 Gallagher, T. M., & Sheldon, N. D. (2013). A new paleothermometer for forest paleosols and its

1251   implications for Cenozoic climate. *Geology*, *41*(6), 647–650.

1252   https://doi.org/10.1130/G34074.1

1253 Ghosh, P., Adkins, J., Affek, H., Balta, B., Guo, W., Schauble, E. A., Schrag, D., & Eiler, J. M.

1254   (2006). 13C–18O bonds in carbonate minerals: A new kind of paleothermometer.

1255   *Geochimica et Cosmochimica Acta*, *70*(6), 1439–1456.

1256 Ghosh, P., Garzione, C. N., & Eiler, J. M. (2006). Rapid Uplift of the Altiplano Revealed

1257   Through 13C-18O Bonds in Paleosol Carbonates. *Science*, *311*(5760), 511–515.

1258   https://doi.org/10.1126/science.1119365

1259 Gierlowski-Kordesch, E. H. (2010). Lacustrine carbonates. *Developments in Sedimentology*, *61*,

1260   1–101.

1261 Grauel, A.-L., Hodell, D. A., & Bernasconi, S. M. (2016). Quantitative estimates of tropical

1262   temperature change in lowland Central America during the last 42 ka. *Earth and*

1263   *Planetary Science Letters*, *438*, 37–46. https://doi.org/10.1016/j.epsl.2016.01.001

1264 Gregory-Wodzicki, K. M. (2000). Uplift history of the Central and Northern Andes: A review.

1265   *GSA Bulletin*, *112*(7), 1091–1105. https://doi.org/10.1130/0016-

1266   7606(2000)112<1091:UHOTCA>2.0.CO;2

1267 Gwynn, J. W. (2007). *Great Salt Lake Brine Chemistry Databases and Reports, 1966-2006*. Utah

1268   Geological Survey Salt Lake City, UT.

1269 Hansen, J., Satoa, M., Kharechaa, P., Beerlingc, D., Bernerd, R., Masson-delmottee, V., Paganid,

1270   M., Raymof, M., Royerg, D. L., & Zachosh, J. C. (2008). *Target Atmospheric CO2:*

1271   *Where Should Humanity Aim?" The Open Atmospheric Science Journal.*

1272 Henkes, G. A., Passey, B. H., Wanamaker Jr, A. D., Grossman, E. L., Ambrose Jr, W. G., &

1273   Carroll, M. L. (2013). Carbonate clumped isotope compositions of modern marine

1274   mollusk and brachiopod shells. *Geochimica et Cosmochimica Acta*, *106*, 307–325.

1275 Hill, P. S., Tripati, A. K., & Schauble, E. A. (2014). Theoretical constraints on the effects of pH,

1276   salinity, and temperature on clumped isotope signatures of dissolved inorganic carbon

1277   species and precipitating carbonate minerals. *Geochimica et Cosmochimica Acta*, *125*,

1278   610–652. https://doi.org/10.1016/j.gca.2013.06.018

1279 Horton, T. W., Defliese, W. F., Tripati, A. K., & Oze, C. (2016). Evaporation induced 18O and

1280   13C enrichment in lake systems: A global perspective on hydrologic balance effects.

1281   *Quaternary Science Reviews*, *131*, 365–379.

1282   https://doi.org/10.1016/j.quascirev.2015.06.030

1283 Hren, M. T., & Sheldon, N. D. (2012). Temporal variations in lake water temperature:

1284   Paleoenvironmental implications of lake carbonate δ18O and temperature records. *Earth*

1285   *and Planetary Science Letters*, *337*, 77–84.

1286   Hren, M. T., Sheldon, N. D., Grimes, S. T., Collinson, M. E., Hooker, J. J., Bugler, M., &

1287   Lohmann, K. C. (2013). Terrestrial cooling in Northern Europe during the Eocene–

1288   Oligocene transition. *Proceedings of the National Academy of Sciences*, *110*(19), 7562–

1289   7567.

1290   Hudson, A. M., Quade, J., Ali, G., Boyle, D., Bassett, S., Huntington, K. W., De los Santos, M.

1291   G., Cohen, A. S., Lin, K., & Wang, X. (2017). Stable C, O and clumped isotope

1292   systematics and 14C geochronology of carbonates from the Quaternary Chewaucan

1293   closed-basin lake system, Great Basin, USA: Implications for paleoenvironmental

1294   reconstructions using carbonates. *Geochimica et Cosmochimica Acta*, *212*, 274–302.

1295   https://doi.org/10.1016/j.gca.2017.06.024

1296   Huntington, K. W., & Lechler, A. R. (2015). Carbonate clumped isotope thermometry in

1297   continental tectonics. *Tectonophysics*, *647–648*, 1–20.

1298   https://doi.org/10.1016/j.tecto.2015.02.019

1299   Huntington, K. W., Saylor, J., Quade, J., & Hudson, A. M. (2015). High late Miocene–Pliocene

1300   elevation of the Zhada Basin, southwestern Tibetan Plateau, from carbonate clumped

1301   isotope thermometry. *Geological Society of America Bulletin*, *127*(1–2), 181–199.

1302   https://doi.org/10.1130/B31000.1

1303   Huntington, K. W., Wernicke, B. P., & Eiler, J. M. (2010). Influence of climate change and uplift

1304   on Colorado Plateau paleotemperatures from carbonate clumped isotope thermometry:

1305   COLORADO PLATEAU CARBONATES. *Tectonics*, *29*(3).

1306   https://doi.org/10.1029/2009TC002449

1307   Ibarra, D. E., Egger, A. E., Weaver, K. L., Harris, C. R., & Maher, K. (2014). Rise and fall of

1308   late Pleistocene pluvial lakes in response to reduced evaporation and precipitation:

1309   Evidence from Lake Surprise, California. *GSA Bulletin*, *126*(11–12), 1387–1415.

1310   https://doi.org/10.1130/B31014.1

1311   Ibarra, D. E., Oster, J. L., Winnick, M. J., Caves Rugenstein, J. K., Byrne, M. P., & Chamberlain,

1312   C. P. (2018). Warm and cold wet states in the western United States during the Pliocene–

1313   Pleistocene. *Geology*, *46*(4), 355–358.

1314   Ingalls, M., Rowley, D., Olack, G., Currie, B., Li, S., Schmidt, J., Tremblay, M., Polissar, P.,

1315   Shuster, D. L., Lin, D., & Colman, A. (2017). Paleocene to Pliocene low-latitude, high-

1316   elevation basins of southern Tibet: Implications for tectonic models of India-Asia

1317   collision, Cenozoic climate, and geochemical weathering. *GSA Bulletin*, *130*(1–2), 307–

1318   330. https://doi.org/10.1130/B31723.1

1319   John, C. M., & Bowen, D. (2016). Community software for challenging isotope analysis: First

1320   applications of 'Easotope' to clumped isotopes: Community software for challenging

1321   isotope analysis. *Rapid Communications in Mass Spectrometry*, *30*(21), 2285–2300.

1322   https://doi.org/10.1002/rcm.7720

1323   Jones, M. D., Roberts, C. N., & Leng, M. J. (2007). Quantifying climatic change through the last

1324   glacial–interglacial transition based on lake isotope palaeohydrology from central

1325   Turkey. *Quaternary Research*, *67*(3), 463–473.

1326   Kato, H., Amekawa, S., Kano, A., Mori, T., Kuwahara, Y., & Quade, J. (2019). Seasonal

1327   temperature changes obtained from carbonate clumped isotopes of annually laminated

1328   tufas from Japan: Discrepancy between natural and synthetic calcites. *Geochimica et*

1329   *Cosmochimica Acta*, *244*, 548–564. https://doi.org/10.1016/j.gca.2018.10.016

1330   Kaufman, D., McKay, N., Routson, C., Erb, M., Davis, B., Heiri, O., Jaccard, S., Tierney, J.,

1331   Dätwyler, C., & Axford, Y. (2020). A global database of Holocene paleotemperature

1332   records. *Scientific Data*, *7*(1), 1–34.

1333   Kele, S., Breitenbach, S. F. M., Capezzuoli, E., Meckler, A. N., Ziegler, M., Millan, I. M.,

1334   Kluge, T., Deák, J., Hanselmann, K., John, C. M., Yan, H., Liu, Z., & Bernasconi, S. M.

1335   (2015). Temperature dependence of oxygen- and clumped isotope fractionation in

1336   carbonates: A study of travertines and tufas in the 6–95°C temperature range.

1337   *Geochimica et Cosmochimica Acta*, *168*, 172–192.

1338   https://doi.org/10.1016/j.gca.2015.06.032

1339   Kelts, K., & Hsü, K. J. (1978). Freshwater Carbonate Sedimentation. In A. Lerman (Ed.), *Lakes:*

1340   *Chemistry, Geology, Physics* (pp. 295–323). Springer New York.

1341   https://doi.org/10.1007/978-1-4757-1152-3_9

1342   Kim, S.-T., & O'Neil, J. R. (1997). Equilibrium and nonequilibrium oxygen isotope effects in

1343   synthetic carbonates. *Geochimica et Cosmochimica Acta*, *61*(16), 3461–3475.

1344   https://doi.org/10.1016/S0016-7037(97)00169-5

1345   Kim, S.-T., O'Neil, J. R., Hillaire-Marcel, C., & Mucci, A. (2007). Oxygen isotope fractionation

1346   between synthetic aragonite and water: Influence of temperature and Mg2+

1347   concentration. *Geochimica et Cosmochimica Acta*, *71*(19), 4704–4715.

1348   https://doi.org/10.1016/j.gca.2007.04.019

1349   Kimball, J., Eagle, R., & Dunbar, R. (2016). Carbonate "clumped" isotope signatures in

1350   aragonitic scleractinian and calcitic gorgonian deep-sea corals. *Biogeosciences*, *13*(23),

1351   6487–6505. https://doi.org/10.5194/bg-13-6487-2016

1352   Kluge, T., Affek, H. P., Zhang, Y. G., Dublyansky, Y., Spötl, C., Immenhauser, A., & Richter,

1353   D. K. (2014). Clumped isotope thermometry of cryogenic cave carbonates. *Geochimica*

1354   *et Cosmochimica Acta*, *126*, 541–554.

1355   Li, H., Liu, X., Arnold, A., Elliott, B., Flores, R., Kelley, A. M., & Tripati, A. (2021). Mass 47

1356   clumped isotope signatures in modern lacustrine authigenic carbonates in Western China

1357   and other regions and implications for paleotemperature and paleoelevation

1358   reconstructions. *Earth and Planetary Science Letters*, *562*, 116840.

1359   https://doi.org/10.1016/j.epsl.2021.116840

1360   Li, H., Liu, X., Tripati, A., Feng, S., Elliott, B., Whicker, C., Arnold, A., & Kelley, A. M.

1361   (2020). Factors controlling the oxygen isotopic composition of lacustrine authigenic

1362   carbonates in Western China: Implications for paleoclimate reconstructions. *Scientific*

1363   *Reports*, *10*(1), 16370. https://doi.org/10.1038/s41598-020-73422-4

1364   Li, L., Fan, M., Davila, N., Jesmok, G., Mitsunaga, B., Tripati, A., & Orme, D. (2019).

1365   Carbonate stable and clumped isotopic evidence for late Eocene moderate to high

1366   elevation of the east-central Tibetan Plateau and its geodynamic implications. *GSA*

1367   *Bulletin*, *131*(5–6), 831–844. https://doi.org/10.1130/B32060.1

1368   Linacre, E. T. (1993). Data-sparse estimation of lake evaporation, using a simplified Penman

1369   equation. *Agricultural and Forest Meteorology*, *64*(3–4), 237–256.

1370   MacDonald, R. (1996). *Baseline physical, biological and chemical parameters of 21 lakes,*

1371   *Togiak National Wildlife Refuge, 1984-1990*. Togiak National Wildlife Refuge, US Fish

1372   and Wildlife Service.

1373   Marić, I., Šiljeg, A., Cukrov, N., Roland, V., & Domazetović, F. (2020). How fast does tufa

1374   grow? Very high-resolution measurement of the tufa growth rate on artificial substrates

1375   by the development of a contactless image-based modelling device. *Earth Surface*

1376   *Processes and Landforms*, *45*(10), 2331–2349. https://doi.org/10.1002/esp.4883

1377 McElwain, J. C. (2004). Climate-independent paleoaltimetry using stomatal density in fossil

1378   leaves as a proxy for CO2 partial pressure. *Geology*, *32*(12), 1017–1020.

1379   https://doi.org/10.1130/G20915.1

1380 McGee, D., Moreno-Chamarro, E., Marshall, J., & Galbraith, E. D. (2018). Western US lake

1381   expansions during Heinrich stadials linked to Pacific Hadley circulation. *Science*

1382   *Advances*, *4*(11), eaav0118.

1383 Meckler, A. N., Vonhof, H., & Martínez-García, A. (2021). Temperature Reconstructions Using

1384   Speleothems. *Elements*, *17*(2), 101–106. https://doi.org/10.2138/gselements.17.2.101

1385 Mering, J. A. (2015). *New constraints on water temperature at Lake Bonneville from carbonate*

1386   *clumped isotopes*. University of California, Los Angeles.

1387 Müller, I. A., Rodriguez-Blanco, J. D., Storck, J.-C., do Nascimento, G. S., Bontognali, T. R. R.,

1388   Vasconcelos, C., Benning, L. G., & Bernasconi, S. M. (2019). Calibration of the oxygen

1389   and clumped isotope thermometers for (proto-)dolomite based on synthetic and natural

1390   carbonates. *Chemical Geology*, *525*, 1–17.

1391   https://doi.org/10.1016/j.chemgeo.2019.07.014

1392 Oviatt, C. G., Habiger, G. D., & Hay, J. E. (1994). Variation in the composition of Lake

1393   Bonneville marl: A potential key to lake-level fluctuations and paleoclimate. *Journal of*

1394   *Paleolimnology*, *11*(1), 19–30. https://doi.org/10.1007/BF00683268

1395 Pace, A., Bourillot, R., Bouton, A., Vennin, E., Galaup, S., Bundeleva, I., Patrier, P., Dupraz, C.,

1396   Thomazo, C., Sansjofre, P., Yokoyama, Y., Franceschi, M., Anguy, Y., Pigot, L.,

1397   Virgone, A., & Visscher, P. T. (2016). Microbial and diagenetic steps leading to the

1398   mineralisation of Great Salt Lake microbialites. *Scientific Reports*, *6*(1), 31495.

1399   https://doi.org/10.1038/srep31495

1400 Pacton, M., Hunger, G., Martinuzzi, V., Cusminsky, G., Burdin, B., Barmettler, K., Vasconcelos,

1401   C., & Ariztegui, D. (2015). Organomineralization processes in freshwater stromatolites:

1402   A living example from eastern Patagonia. *The Depositional Record*, *1*(2), 130–146.

1403   https://doi.org/10.1002/dep2.7

1404 Passey, B. H., Levin, N. E., Cerling, T. E., Brown, F. H., & Eiler, J. M. (2010). High-

1405   temperature environments of human evolution in East Africa based on bond ordering in

1406   paleosol carbonates. *Proceedings of the National Academy of Sciences*, *107*(25), 11245–

1407   11249. https://doi.org/10.1073/pnas.1001824107

1408 Pedley, H. M. (1990). Classification and environmental models of cool freshwater tufas.

1409   *Sedimentary Geology*, *68*(1–2), 143–154.

1410 Pedone, V. A. (2002). Oxygen-isotope composition of Great Salt Lake, 1979 to 1996. *Great Salt*

1411   *Lake: An Overview of Change*, 121–126.

1412 Pérez, L., Bugja, R., Lorenschat, J., Brenner, M., Curtis, J., Hoelzmann, P., Islebe, G., Scharf, B.,

1413   & Schwalb, A. (2011). Aquatic ecosystems of the Yucatan peninsula (Mexico), Belize,

1414   and Guatemala. *Hydrobiologia*, *661*(1), 407–433.

1415 Petersen, S. V., Defliese, W. F., Saenger, C., Daëron, M., Huntington, K. W., John, C. M.,

1416   Kelson, J. R., Bernasconi, S. M., Colman, A. S., Kluge, T., Olack, G. A., Schauer, A. J.,

1417   Bajnai, D., Bonifacie, M., Breitenbach, S. F. M., Fiebig, J., Fernandez, A. B., Henkes, G.

1418   A., Hodell, D., … Winkelstern, I. Z. (2019). Effects of Improved 17O Correction on

1419   Interlaboratory Agreement in Clumped Isotope Calibrations, Estimates of Mineral-

1420   Specific Offsets, and Temperature Dependence of Acid Digestion Fractionation.

1421   *Geochemistry, Geophysics, Geosystems*, *20*(7), 3495–3519.

1422   https://doi.org/10.1029/2018GC008127

1423   Petryshyn, V. A., Juarez Rivera, M., Agić, H., Frantz, C. M., Corsetti, F. A., & Tripati, A. E.

1424   (2016). Stromatolites in Walker Lake (Nevada, Great Basin, USA) record climate and

1425   lake level changes ~35,000years ago. *Palaeogeography, Palaeoclimatology,*

1426   *Palaeoecology*, *451*, 140–151. https://doi.org/10.1016/j.palaeo.2016.02.054

1427   Petryshyn, V. A., Lim, D., Laval, B. L., Brady, A., Slater, G., & Tripati, A. K. (2015).

1428   Reconstruction of limnology and microbialite formation conditions from carbonate

1429   clumped isotope thermometry. *Geobiology*, *13*(1), 53–67.

1430   https://doi.org/10.1111/gbi.12121

1431   Phillips, K. N., & Van Denburgh, A. S. (1971). *Hydrology and geochemistry of Abert, Summer,*

1432   *and Goose Lakes and other closed-basin lakes in south-central Oregon*. US Government

1433   Printing Office.

1434   Piovano, E. L., Ariztegui, D., Bernasconi, S. M., & McKenzie, J. A. (2004). Stable isotopic

1435   record of hydrological changes in subtropical Laguna Mar Chiquita (Argentina) over the

1436   last 230 years. *The Holocene*, *14*(4), 525–535.

1437   Platt, N. H., & Wright, V. P. (2009). Lacustrine Carbonates: Facies Models, Facies Distributions

1438   and Hydrocarbon Aspects. In *Lacustrine Facies Analysis* (pp. 57–74). John Wiley &

1439   Sons, Ltd. https://doi.org/10.1002/9781444303919.ch3

1440   Poage, M. A., & Chamberlain, C. P. (2001). Empirical Relationships Between Elevation and the

1441   Stable Isotope Composition of Precipitation and Surface Waters: Considerations for

1442   Studies of Paleoelevation Change. *American Journal of Science*, *301*(1), 1–15.

1443   https://doi.org/10.2475/ajs.301.1.1

1444 Powers, L., Werne, J. P., Vanderwoude, A. J., Sinninghe Damsté, J. S., Hopmans, E. C., &

1445   Schouten, S. (2010). Applicability and calibration of the TEX86 paleothermometer in

1446   lakes. *Organic Geochemistry*, *41*(4), 404–413.

1447   https://doi.org/10.1016/j.orggeochem.2009.11.009

1448 Quade, J., Eiler, J., Daëron, M., & Achyuthan, H. (2013). The clumped isotope geothermometer

1449   in soil and paleosol carbonate. *Geochimica et Cosmochimica Acta*, *105*, 92–107.

1450   https://doi.org/10.1016/j.gca.2012.11.031

1451 R Core Team. (2022). *R: A language and environment for statistical computing.* R Foundation

1452   for Statistical Computing. https://www.R-project.org/

1453 Reati, G. J., Florín, M., Fernández, G. J., & Montes, C. (1996). The Laguna de Mar Chiquita

1454   (Córdoba, Argentina): A little known, secularly fluctuating, saline lake. *International*

1455   *Journal of Salt Lake Research*, *5*(3), 187–219. https://doi.org/10.1007/BF01997137

1456 Román Palacios, C., Carroll, H., Arnold, A., Flores, R., Petersen, S., McKinnon, K., & Tripati,

1457   A. (2021). *BayClump: Bayesian Calibration and Temperature Reconstructions for*

1458   *Clumped Isotope Thermometry*. https://www.essoar.org/doi/10.1002/essoar.10507995.1

1459 Rowley, D. B., & Garzione, C. N. (2007). Stable Isotope-Based Paleoaltimetry. *Annual Review*

1460   *of Earth and Planetary Sciences*, *35*(1), 463–508.

1461   https://doi.org/10.1146/annurev.earth.35.031306.140155

1462 Roy, P. D., Charles-Polo, M. P., Lopez-Balbiaux, N., Pi-Puig, T., Sankar, G. M., Lozano-

1463   Santacruz, R., Lozano-García, S., & Romero, F. M. (2014). Last glacial hydrological

1464   variations at the southern margin of sub-tropical North America and a regional

1465   comparison. *Journal of Quaternary Science*, *29*(5), 495–505.

1466   https://doi.org/10.1002/jqs.2718

1467   Roy, P. D., Rivero-Navarette, A., Lopez-Balbiaux, N., Pérez-Cruz, L. L., Metcalfe, S. E., Sankar,

1468   G. M., & Sánchez-Zavala, J. L. (2013). A record of Holocene summer-season

1469   palaeohydrological changes from the southern margin of Chihuahua Desert (Mexico) and

1470   possible forcings. *The Holocene*, *23*(8), 1105–1114.

1471   https://doi.org/10.1177/0959683613483619

1472   Roy, P. D., Rivero-Navarrete, A., Sánchez-Zavala, J. L., Beramendi-Orosco, L. E., Muthu-

1473   Sankar, G., & Lozano-Santacruz, R. (2016). Atlantic Ocean modulated hydroclimate of

1474   the subtropical northeastern Mexico since the last glacial maximum and comparison with

1475   the southern US. *Earth and Planetary Science Letters*, *434*, 141–150.

1476   https://doi.org/10.1016/j.epsl.2015.11.048

1477   Roy, R., Wang, Y., & Jiang, S. (2019). Growth pattern and oxygen isotopic systematics of

1478   modern freshwater mollusks along an elevation transect: Implications for paleoclimate

1479   reconstruction. *Palaeogeography, Palaeoclimatology, Palaeoecology*, *532*, 109243.

1480   https://doi.org/10.1016/j.palaeo.2019.109243

1481   Saenger, C., Affek, H. P., Felis, T., Thiagarajan, N., Lough, J. M., & Holcomb, M. (2012).

1482   Carbonate clumped isotope variability in shallow water corals: Temperature dependence

1483   and growth-related vital effects. *Geochimica et Cosmochimica Acta*, *99*, 224–242.

1484   https://doi.org/10.1016/j.gca.2012.09.035

1485   Santi, L., Ibarra, D. E., Mering, J., Arnold, A., Tripati, A., Whicker, C., & Oviatt, C. G. (2019).

1486   *Lake level fluctuations in the Northern Great Basin for the last 25,000 years.*

1487   Santi, L. M., Arnold, A. J., Ibarra, D. E., Whicker, C. A., Mering, J. A., Lomarda, R. B., Lora, J.

1488   M., & Tripati, A. (2020). Clumped isotope constraints on changes in latest Pleistocene

1489   hydroclimate in the northwestern Great Basin: Lake Surprise, California. *GSA Bulletin*,

1490   *132*(11–12), 2669–2683.

1491 Schauble, E. A., Ghosh, P., & Eiler, J. M. (2006). Preferential formation of 13C–18O bonds in

1492   carbonate minerals, estimated using first-principles lattice dynamics. *Geochimica et*

1493   *Cosmochimica Acta*, *70*(10), 2510–2529. https://doi.org/10.1016/j.gca.2006.02.011

1494 Solari, M. A., Hervé, F., Le Roux, J. P., Airo, A., & Sial, A. N. (2010). Paleoclimatic

1495   significance of lacustrine microbialites: A stable isotope case study of two lakes at Torres

1496   del Paine, southern Chile. *Palaeogeography, Palaeoclimatology, Palaeoecology*, *297*(1),

1497   70–82. https://doi.org/10.1016/j.palaeo.2010.07.016

1498 Spencer, C., & Kim, S.-T. (2015). Carbonate clumped isotope paleothermometry: A review of

1499   recent advances in CO2 gas evolution, purification, measurement and standardization

1500   techniques. *Geosciences Journal*, *19*(2), 357–374. https://doi.org/10.1007/s12303-015-

1501   0018-1

1502 Spooner, P. T., Guo, W., Robinson, L. F., Thiagarajan, N., Hendry, K. R., Rosenheim, B. E., &

1503   Leng, M. J. (2016). Clumped isotope composition of cold-water corals: A role for vital

1504   effects? *Geochimica et Cosmochimica Acta*, *179*, 123–141.

1505 Stephens, J. C. (1977). Hydrologic Reconnaissance of the Tule Valley Drainage Basin, Juab and

1506   Millard Counties, Utah. *State of Utah, Department of Natural Resources*, *Technical*

1507   *Publication No. 56.*

1508 Street-Perrott, F. A., & Harrison, S. P. (2013). Temporal Variations in Lake Levels Since 30,000

1509   YR BP—An Index of the Global Hydrological Cycle. In *Climate Processes and Climate*

1510   *Sensitivity* (pp. 118–129). American Geophysical Union (AGU).

1511   https://doi.org/10.1029/GM029p0118

1512   Stuiver, M., & Grootes, P. M. (2000). GISP2 oxygen isotope ratios. *Quaternary Research*, *53*(3),

1513   277–284.

1514   Stute, M., & Schlosser, P. (2000). Atmospheric Noble Gases. In P. G. Cook & A. L. Herczeg

1515   (Eds.), *Environmental Tracers in Subsurface Hydrology* (pp. 349–377). Springer US.

1516   https://doi.org/10.1007/978-1-4615-4557-6_11

1517   Swart, P. K., Burns, S. J., & Leder, J. J. (1991). Fractionation of the stable isotopes of oxygen

1518   and carbon in carbon dioxide during the reaction of calcite with phosphoric acid as a

1519   function of temperature and technique. *Chemical Geology: Isotope Geoscience Section*,

1520   *86*(2), 89–96.

1521   Tang, J., Dietzel, M., Fernandez, A., Tripati, A. K., & Rosenheim, B. E. (2014). Evaluation of

1522   kinetic effects on clumped isotope fractionation ($\Delta 47$) during inorganic calcite

1523   precipitation. *Geochimica et Cosmochimica Acta*, *134*, 120–136.

1524   https://doi.org/10.1016/j.gca.2014.03.005

1525   Tierney, J. E., & Russell, J. M. (2009). Distributions of branched GDGTs in a tropical lake

1526   system: Implications for lacustrine application of the MBT/CBT paleoproxy. *Organic

1527   Geochemistry*, *40*(9), 1032–1036.

1528   Tripati, A. K., Eagle, R. A., Thiagarajan, N., Gagnon, A. C., Bauch, H., Halloran, P. R., & Eiler,

1529   J. M. (2010). 13C–18O isotope signatures and 'clumped isotope' thermometry in

1530   foraminifera and coccoliths. *Geochimica et Cosmochimica Acta*, *74*(20), 5697–5717.

1531   https://doi.org/10.1016/j.gca.2010.07.006

1532   Tripati, A. K., Hill, P. S., Eagle, R. A., Mosenfelder, J. L., Tang, J., Schauble, E. A., Eiler, J. M.,

1533   Zeebe, R. E., Uchikawa, J., Coplen, T. B., Ries, J. B., & Henry, D. (2015). Beyond

1534   temperature: Clumped isotope signatures in dissolved inorganic carbon species and the

1535   influence of solution chemistry on carbonate mineral composition. *Geochimica et*

1536   *Cosmochimica Acta*, *166*, 344–371. https://doi.org/10.1016/j.gca.2015.06.021

1537   Tripati, A. K., Sahany, S., Pittman, D., Eagle, R. A., Neelin, J. D., Mitchell, J. L., & Beaufort, L.

1538   (2014). Modern and glacial tropical snowlines controlled by sea surface temperature and

1539   atmospheric mixing. *Nature Geoscience*, *7*(3), 205–209.

1540   https://doi.org/10.1038/ngeo2082

1541   Upadhyay, D., Lucarelli, J., Arnold, A., Flores, R., Bricker, H., Ulrich, R. N., Jesmok, G., Santi,

1542   L., Defliese, W., Eagle, R. A., Carroll, H. M., Bateman, J. B., Petryshyn, V., Loyd, S. J.,

1543   Tang, J., Priyadarshi, A., Elliott, B., & Tripati, A. (2021). Carbonate clumped isotope

1544   analysis ($\Delta 47$) of 21 carbonate standards determined via gas-source isotope-ratio mass

1545   spectrometry on four instrumental configurations using carbonate-based standardization

1546   and multiyear data sets. *Rapid Communications in Mass Spectrometry*, *35*(17), e9143.

1547   https://doi.org/10.1002/rcm.9143

1548   Urey, H. C. (1947). The thermodynamic properties of isotopic substances. *Journal of the*

1549   *Chemical Society (Resumed)*, *0*, 562–581. https://doi.org/10.1039/JR9470000562

1550   U.S. Geological Survey. (2022a). *National Water Information System data available on the*

1551   *World Wide Web (USGS Water Data for the Nation)*. OAK CREEK AT RED ROCK

1552   CROSSING NR SEDONA, AZ (USGS-09504440) Site Data in the Water Quality Portal.

1553   https://www.waterqualitydata.us/provider/NWIS/USGS-AZ/USGS-09504440/

1554   U.S. Geological Survey. (2022b). *National Water Information System data available on the*

1555   *World Wide Web (USGS Water Data for the Nation)*. USGS 11042510 VAIL LK NR

1556   TEMECULA CA.

1557   https://waterdata.usgs.gov/nwis/inventory/?site_no=11042510&agency_cd=USGS

1558 U.S. Geological Survey. (2022c). *National Water Information System data available on the*

1559 *World Wide Web (USGS Water Data for the Nation)*. USGS 09522000 COLORADO

1560 RIVER AT NIB, ABOVE MORELOS DAM, AZ.

1561 https://waterdata.usgs.gov/nwis/inventory/?site_no=09522000

1562 U.S. Geological Survey. (2022d). *National Water Information System data available on the*

1563 *World Wide Web (USGS Water Data for the Nation)*. SANTA CLARA RIVER ABV

1564 BAKER RES, NR CENTRAL, UT (USGS-09409100).

1565 https://www.waterqualitydata.us/provider/NWIS/USGS-UT/USGS-09409100/

1566 USDA Natural Resources Conservation Service. (2022). *SNOwpack TELemetry Network*

1567 *(SNOTEL)*. SNOwpack TELemetry Network (SNOTEL).

1568 https://data.nal.usda.gov/dataset/snowpack-telemetry-network-snotel.

1569 van Dijk, J., Fernandez, A., Storck, J. C., White, T. S., Lever, M., Müller, I. A., Bishop, S.,

1570 Seifert, R. F., Driese, S. G., Krylov, A., Ludvigson, G. A., Turchyn, A. V., Lin, C. Y.,

1571 Wittkop, C., & Bernasconi, S. M. (2019). Experimental calibration of clumped isotopes

1572 in siderite between 8.5 and 62 °C and its application as paleo-thermometer in paleosols.

1573 *Geochimica et Cosmochimica Acta*, *254*, 1–20. https://doi.org/10.1016/j.gca.2019.03.018

1574 Vasconcelos, C., McKenzie, J. A., Warthmann, R., & Bernasconi, S. M. (2005). Calibration of

1575 the δ18O paleothermometer for dolomite precipitated in microbial cultures and natural

1576 environments. *Geology*, *33*(4), 317–320. https://doi.org/10.1130/G20992.1

1577 Velázquez, N. I. T. (2017). Paleohydrology record of the stromatolites of the Bacalar Lagoon:

1578 New insight for climate change assessment in the Mexican Caribbean. *XVI World Water*

1579 *Congress*.

1580   Versteegh, E. A., Vonhof, H. B., Troelstra, S. R., Kaandorp, R. J., & Kroon, D. (2010).

1581   Seasonally resolved growth of freshwater bivalves determined by oxygen and carbon

1582   isotope shell chemistry. *Geochemistry, Geophysics, Geosystems*, *11*(8).

1583   Wang, Y., Passey, B., Roy, R., Deng, T., Jiang, S., Hannold, C., Wang, X., Lochner, E., &

1584   Tripati, A. (2021). Clumped isotope thermometry of modern and fossil snail shells from

1585   the Himalayan-Tibetan Plateau: Implications for paleoclimate and paleoelevation

1586   reconstructions. *GSA Bulletin*, *133*(7–8), 1370–1380. https://doi.org/10.1130/B35784.1

1587   Wilbur, K. M., & Watabe, N. (1963). Experimental Studies on Calcification in Molluscs and the

1588   Alga Coccolithus Huxleyi. *Annals of the New York Academy of Sciences*, *109*(1), 82–112.

1589   https://doi.org/10.1111/j.1749-6632.1963.tb13463.x

1590   Wilf, P. (1997). When are leaves good thermometers? A new case for Leaf Margin Analysis.

1591   *Paleobiology*, *23*(3), 373–390. https://doi.org/10.1017/S0094837300019746

1592   Willmott, Cort J., & Matsuura, K. (2001). *Terrestrial Air Temperature and Precipitation:*

1593   *Monthly and Annual Time Series (1950—1999).*

1594   http://climate.geog.udel.edu/~climate/html_pages/README.ghcn_ts2.html

1595   Wolfe, J. A., Forest, C. E., & Molnar, P. (1998). Paleobotanical evidence of Eocene and

1596   Oligocene paleoaltitudes in midlatitude western North America. *GSA Bulletin*, *110*(5),

1597   664–678. https://doi.org/10.1130/0016-7606(1998)110<0664:PEOEAO>2.3.CO;2

1598   Wrozyna, C., Meyer, J., Dietzel, M., & Piller, W. E. (2022). Neotropical ostracode oxygen and

1599   carbon isotope signatures: Implications for calcification conditions. *Biogeochemistry*,

1600   *159*(1), 103–138. https://doi.org/10.1007/s10533-022-00917-9

1601   Xu, H., Ai, L., Tan, L., & An, Z. (2006). Stable isotopes in bulk carbonates and organic matter in

1602   recent sediments of Lake Qinghai and their climatic implications. *Chemical Geology*,

1603   *235*(3), 262–275. https://doi.org/10.1016/j.chemgeo.2006.07.005

1604   Yu, S., Liu, J., Xu, J., & Wang, H. (2011). Evaporation and energy balance estimates over a

1605   large inland lake in the Tibet-Himalaya. *Environmental Earth Sciences*, *64*(4), 1169–

1606   1176.

1607   Yuan, F., Linsley, B. K., & Howe, S. S. (2006). Evaluating sedimentary geochemical lake-level

1608   tracers in Walker Lake, Nevada, over the last 200 years. *Journal of Paleolimnology*,

1609   *36*(1), 37–54.

1610   Zaarur, S., Affek, H. P., & Brandon, M. T. (2013). A revised calibration of the clumped isotope

1611   thermometer. *Earth and Planetary Science Letters*, *382*, 47–57.

1612   https://doi.org/10.1016/j.epsl.2013.07.026

1613